

Ab initio calculations of the atomic and electronic structures for ABO_3 perovskite (001) surfaces

S. Piskunov^{a,b}, E. A. Kotomin^b, E. Heifets^c

May 7, 2004

^aFachbereich Physik, Universität Osnabrück, D-49069 Osnabrück, Germany

^bInstitute of Solid State Physics, University of Latvia, Kengaraga 8, LV- 1063 Riga, Latvia

^cCalifornia Institute of Technology, MS 139-74, Pasadena CA 91125, USA

Abstract

We present the results of first-principles calculations on two possible terminations of the (001) surfaces of SrTiO_3 (STO), BaTiO_3 (BTO), and PbTiO_3 (PTO) perovskite crystals. Atomic structure and the electronic configurations were calculated for different 2D slabs, both stoichiometric and non-stoichiometric, using *hybrid* (B3PW) exchange-correlation technique and re-optimized basis sets of atomic (Gaussian) orbitals. Results are compared with previous calculations and available experimental data. The electronic density distribution near the surface and covalency effects are discussed in details for all three perovskites.

Key words: SrTiO_3 , BaTiO_3 , PbTiO_3 , single crystal surfaces, surface relaxation, atomic and electronic structure, *ab initio* calculations

1 Introduction

The ABO_3 perovskite surfaces are important for many technological applications, *e.g.* STO is widely used as a substrate for epitaxial growth of high- T_c superconducting thin films, BTO and PTO and their solid solutions are promising for non-volatile memory cells, as electro-optical materials, and for piezoelectrical devices [1, 2, 3, 4]. Due to intensive development and progressive miniaturization of electronic devices, the electronic properties and atomic structure of the ABO_3 perovskite thin films were extensively studied during the last years. The STO(001) surface structure

was analyzed by means of Low Energy Electron Diffraction (LEED) [5], Reflection High Energy Electron Diffraction (RHEED), X-ray Photoelectron Spectroscopy (XPS) and Ultraviolet Electron Spectroscopy (UPS) [6], Medium Energy Ion Scattering (MEIS) [7], and Surface X-ray Diffraction (SXRD) [8]. The most recent experimental studies on the STO(001) include a combination of XPS, LEED, and Time-Of-Flight Scattering and Recoiling Spectrometry (TOF-SARS) [9], and UPS and Metastable Impact Electron Spectroscopy (MIES) [10]. The BTO and PTO surfaces are less studied. The first *ab initio* calculations of the ABO_3 perovskite surfaces were presented by Kimura *et al.* in 1995 [11]. Since then a number of calculations were performed, using different methods, *e.g.* Linearized Augmented Plane Waves (LAPW) [12, 13], PW ultrasoft-pseudopotential [14, 15, 16, 17], Hartree-Fock (HF) [18]. Recently, new studies on the STO(001) surface relaxation were performed using Density Functional Theory (DFT) with plane wave (PW) basis set (DFT-PW method) [19] and Shell Model (SM) simulations with parameters obtained from first-principles LAPW method [20, 21]. In most of these studies DFT and plane-wave basis sets were used (the only exception is HF study [18]). It is well-known that DFT considerably underestimate the band gap. On the other hand, band gap obtained through the HF calculations is usually an overestimate [22]. To solve this problem, the functionals containing “*hybrid*” of the non-local HF exchange, DFT exchange, and Generalized Gradient Approximation (GGA) correlation functionals, and known as B3LYP and B3PW (which are quite popular in quantum chemistry of molecules) [23, 24] could be used. Recently, periodic-structure *ab initio* hybrid calculations were carried out for wide range of crystalline materials [25], as well as for perovskites and their surfaces [26, 27]. In all cases the hybrid functional technique shows the best agreement with experimental data for both bulk geometry and optical properties of materials under investigation. In this paper we continue our own theoretical investigation of the surfaces of perovskite materials. These have been carried out using both semi-empirical SM [28] and *ab initio* HF and DFT methods [29, 30, 27, 31]. Mostly, these studies are dedicated to STO(001) surfaces. We studied the effects of different type of Hamiltonians (varied from DFT-LDA to HF with *posteriori* corrections) on surfaces properties and atomic structure. This analysis allowed us to choose the B3PW functional as the best for describing the bulk properties of all three perovskites under consideration [26] as well as the basic surface properties [27]. This is why in the present study we use B3PW for comparing the atomic structure and the electronic properties of the (001) surfaces of three similar perovskites, STO, BTO, and PTO. In our simulations, the (001) surfaces of perovskites are calculated using a *slab* model.

The paper is organized as follows: in Section 2 we present the technical details

of calculations and methodology. In Section 3 we discuss the surface structure and the electronic properties of the (001) surfaces. Our conclusions are summarized in Section 4.

2 Computational Details

To perform the first-principles DFT-B3PW calculations, the CRYSTAL’98 computer code [22, 32, 33, 34] was used. This code uses localized Gaussian-type functions (GTF) localized at atoms as the basis for an expansion of the crystalline orbitals. The ability to calculate the electronic structure of materials within both HF and Kohn-Sham (KS) Hamiltonians and implementation of purely 2D slab model without its artificial repetition along the Z axis, are the main advantages of this code. However, in order to employ the LCAO-GTF method, it is desirable to optimize the basis sets (BS), which would be suitable for the electronic structure computations. Such BS’s optimization for all three perovskites is developed and discussed in Ref. [26]. Unlike the standard basis set [33], we added the polarized O d orbitals, replaced the Ti inner core orbitals by the small-core Hay-Wadt pseudopotentials, and consistently used the two diffuse s and p Gaussians as the separate basis orbitals on the Ti, Ba, Sr and Pb.

Our calculations were performed using the hybrid exchange-correlation B3PW functional involving a hybrid of non-local Fock exact exchange and Becke’s three-parameter gradient corrected exchange functional [35] combined with the non-local gradient corrected correlation potential by Perdew and Wang [36, 37, 38]. The Hay-Wadt small-core ECP’s [39, 40, 41] were adopted for Ti, Sr, and Ba atoms [39, 40, 41]. The “small-core” ECP’s replace only inner core orbitals, but orbitals for outer core electrons as well as for valence electrons are calculated self-consistently. Light oxygen atoms were left with the full electron BS. The BSs were adopted in the following forms: O - 8-411(1d)G (the first shell is of s -type and is a contraction of eight Gaussian type functions, then there are three sp -shells and one d -shell), Ti - 411(311d)G, Sr and Ba - 311(1d)G; see Ref. [26] for more details.

The reciprocal space integration was performed by the sampling the Brillouin zone of the unit cell with the $8 \times 8 \times 1$ Pack-Monkhorst net [42], that provides the balanced summation in direct and reciprocal lattices [43]. To achieve high accuracy, large enough tolerances of 7, 8, 7, 7, 14, (i.e. the calculation of integrals with an accuracy of 10^{-N}) were chosen for the Coulomb overlap, Coulomb penetration, exchange overlap, the first exchange pseudo-overlap, and for the second exchange pseudo-overlap respectively [32].

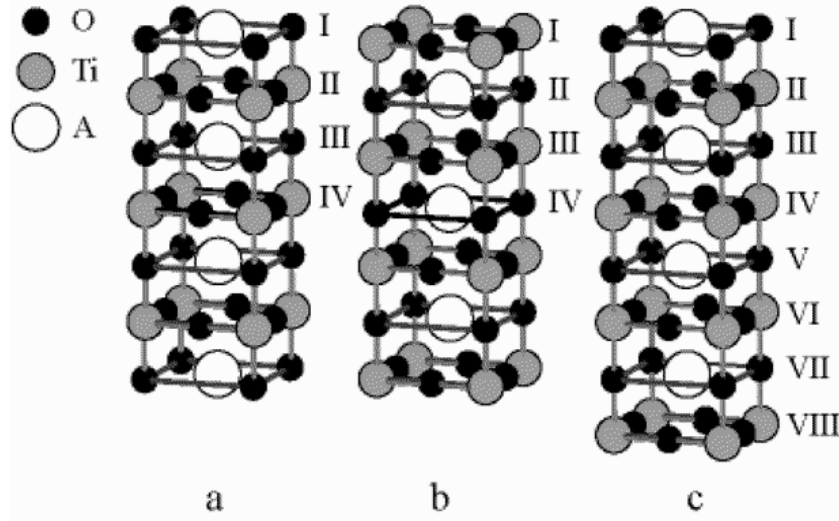


Figure 1: Schematic view of the modelling for $ABO_3(001)$ surfaces: a) AO-terminated on both sides, b) TiO_2 -terminated on both sides, c) asymmetrical termination (AO atop and TiO_2 on bottom).

The $ABO_3(001)$ surfaces were modelled considering the crystal as a set of crystalline planes perpendicular to the given surface, and cutting out 2D slab of a finite thickness, periodic in x - y plane. The symmetrical 7-plane slabs are either AO- or TiO_2 -terminated. These are non-stoichiometric with unit cell formulas $A_4B_3O_{10}$ and $A_3B_4O_{11}$, respectively. Asymmetrical slab is AO- and TiO_2 -terminated (from each side, respectively), and stoichiometric with a formula $A_4B_4O_{12}$ unit cell – are shown schematically in Fig. 1. These slabs containing seven planes (symmetric) and eight planes (asymmetric) can be considered as thick enough since the convergence of calculated slab total energy per ABO_3 unit is achieved. This energy differs less than $5 \cdot 10^{-4}$ Hartree for 7- and 9-layered (or 8- and 10-layered for asymmetrical termination) slabs for all three perovskites. The symmetric slabs have advantage of no dipole moment perpendicular to the slab. However, their non-stoichiometry can potentially affect the electronic density distributions and thus atomic displacements. On the other hand, since the effective atomic charges of Ti and O ions differ from the ionic charges $+4e$, $-2e$ (due to the covalency contribution in Ti-O chemical bonding), the alternating TiO_2 and AO planes are slightly charged, which produces in the asymmetrical slab certain dipole moment perpendicular to the slab. This dipole moment is cancelled by the electronic density redistribution near the surface which also can affect the optimized atomic displacements. This is why a critical comparison of these two slab models is important for making reliable conclusions.

In order to compare surface properties of three perovskites, we study here their

high-symmetry cubic ($Pm\bar{3}m$) phases. The calculated bulk lattice constants (in Å) are: $a = 3.90$ for STO, $a = 4.01$ for BTO, and $a = 3.93$ for PTO, which demonstrates the excellent agreement with experiment [44, 45].

3 Results and Discussions

3.1 Surface Atomic Structure

In present surface structure simulations we allowed atoms of two outermost surface layers to relax along the z axis (by symmetry, surfaces of perfect cubic crystals have no forces along the x - and y -axes). Displacements of third layer atoms were found negligibly small in our calculations and thus are not treated. The optimization of atomic coordinates was done through the slab total energy minimization using our own computer code which implements Conjugated Gradients optimization technique [46] with a numerical computation of derivatives.

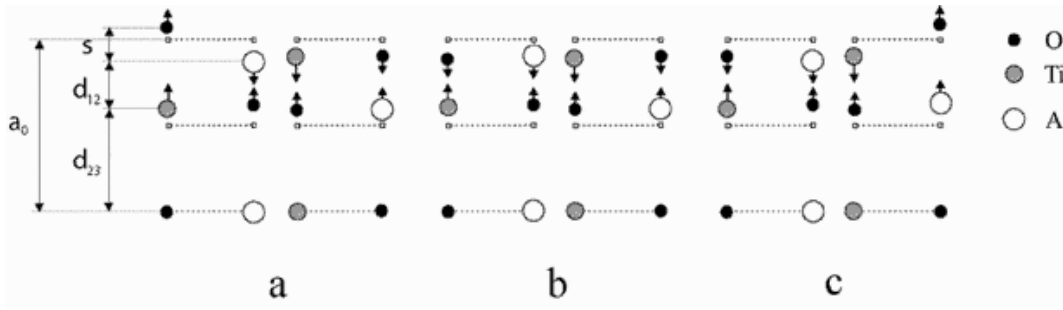


Figure 2: Schematic illustration of the relaxation for two outermost surface layers relaxation: a) STO, b) BTO, c) PTO. The view in the $[010]$ direction. Left panels in a - c are AO termination, right panels – TiO_2 . Dashed lines represent positions of the same layers in perfect bulk crystals.

Our calculated atomic displacements are presented in Table 1 and are schematically illustrated in Fig. 2. A comparison with the surface atomic displacements obtained by other Quantum Mechanical (QM) calculations is also done in Table 1. The relaxation of surface metal atoms is much larger than that of oxygens which leads to a considerable *rumpling* of the outermost plane. Atoms of the first surface layer relax inwards, *i.e.* towards the bulk. The two exceptions are the top oxygens of STO SrO-terminated and PTO TiO_2 -terminated surfaces (the latter PW-pseudopotential calculations are in disagreement [16], however the magnitudes of both displacements are relative small, 0.31 and -0.34 per cents of lattice constant, respectively.) The

Table 1: Atomic displacements with respect to atomic positions on unrelaxed $\text{ABO}_3(001)$ surfaces (in percent of bulk lattice constant). Symbol A can mean Sr, Ba, or Pb atom. Positive displacements are outwards (to the vacuum), negative displacements mean inward the slab center.

| N | At. | STO | | | | | BTO | | | | | PTO | |
|-------------------------------|----------------|------------|-------|-------|------|-------|------------|-------|-------|-------|-------|------------|-------|
| | | This study | [27] | [28] | [15] | [19] | This study | [28] | [14] | [20] | [13] | This Study | [16] |
| AO-termination | | | | | | | | | | | | | |
| 1 | A | -4.84 | -4.29 | -7.10 | -5.7 | -6.66 | -1.99 | -3.72 | -2.79 | -0.72 | | -3.82 | -4.36 |
| | O | 0.84 | 0.61 | 1.15 | 0.1 | 1.02 | -0.63 | 1.00 | -1.40 | -1.09 | | -0.31 | -0.46 |
| 2 | Ti | 1.75 | 1.25 | 1.57 | 1.2 | 1.79 | 1.74 | 1.25 | 0.92 | 1.70 | | 3.07 | 2.39 |
| | O ₂ | 0.77 | 0.85 | 0.87 | 0.0 | 0.26 | 1.40 | 0.76 | 0.48 | 2.75 | | 2.30 | 1.21 |
| 3 | A | | | -1.42 | -1.2 | -1.54 | | -0.51 | 0.53 | -0.69 | | | -1.37 |
| | O | | | 0.7 | -0.1 | 0.26 | | 0.16 | 0.26 | -0.28 | | | -0.20 |
| TiO ₂ -termination | | | | | | | | | | | | | |
| 1 | Ti | -2.25 | -2.19 | -2.96 | -3.4 | -1.79 | -3.08 | -2.72 | -3.89 | -4.14 | | -2.81 | -3.40 |
| | O ₂ | -0.13 | -0.93 | -1.73 | -1.6 | -0.26 | -0.35 | -0.94 | -1.63 | -2.74 | | 0.31 | -0.34 |
| 2 | A | 3.55 | 2.18 | 3.46 | 2.5 | 4.61 | 2.51 | 2.19 | 1.31 | 2.36 | | 5.32 | 4.53 |
| | O | 0.57 | 0.01 | -0.21 | -0.5 | 0.77 | 0.38 | -0.17 | -0.62 | -0.50 | | 1.28 | 0.43 |
| 3 | Ti | | | -0.6 | -0.7 | -0.26 | | -0.33 | -0.75 | -0.81 | | | -0.92 |
| | O ₂ | | | -0.29 | -0.5 | 0.26 | | -0.01 | -0.35 | -0.72 | | | -0.27 |
| asymmetrical termination | | | | | | | | | | | | | |
| 1 | A | -5.22 | | | | | -2.09 | | | -1.8 | -4.28 | -4.02 | |
| | O | 0.39 | | | | | -0.69 | | | -1.98 | -3.26 | -0.24 | |
| 2 | Ti | 1.55 | | | | | 1.70 | | | | | 3.01 | |
| | O ₂ | 0.61 | | | | | 1.50 | | | | | 1.95 | |
| ... | ... | ... | | | | | ... | | | ... | ... | ... | |
| ... | ... | ... | | | | | ... | | | ... | ... | ... | |
| ... | ... | ... | | | | | ... | | | ... | ... | ... | |
| 7 | O | -0.64 | | | | | -0.37 | | | | | -1.22 | |
| | A | -3.74 | | | | | -2.54 | | | | | -5.44 | |
| 8 | O ₂ | 0.15 | | | | | 0.34 | | | 3.52 | 2.68 | -0.74 | |
| | Ti | 2.27 | | | | | 3.03 | | | 4.72 | 4.79 | 2.84 | |

outward relaxation of all atoms in the second layer is found for all three perovskites and both terminations. The displacements obtained for asymmetrically terminated slabs are practically the same as for those symmetrically terminated. This means that both slab models are reliable for the calculations of the (001) neutral surfaces and that 7-8 plane slabs thick enough.

In order to compare the calculated surface structures with available results obtained experimentally, the surface rumpling s (the relative displacement of oxygen with respect to the metal atom in the surface layer) and the changes in interlayer distances Δd_{12} and Δd_{23} (1, 2, and 3 are the numbers of near-surface layers) are presented in Table 2. Our calculations of the interlayer distances are based on the positions of relaxed *metal* ions (Fig. 2), which are known to be much stronger electron scatters than oxygen ions [5]. The agreement is quite good for all theoretical

Table 2: Calculated and experimental surface rumpling s , and relative displacements of the three near-surface planes for the AO- and TiO₂-terminated surfaces Δd_{ij} (in percent of lattice constant). Results for asymmetrical surfaces are given in brackets.

| | | AO-terminated | | | TiO ₂ -terminated | | |
|-----|-----------------------|---------------|-----------------|-----------------|------------------------------|-----------------|-----------------|
| | | s | Δd_{12} | Δd_{23} | s | Δd_{12} | Δd_{23} |
| STO | This study | 5.66 | -6.58 | 1.75 | 2.12 | -5.79 | 3.55 |
| | | (5.61) | (-6.79) | (1.55) | (2.43) | (-6.02) | (3.74) |
| | <i>ab initio</i> [27] | 4.9 | -5.5 | | 1.3 | -4.4 | |
| | <i>ab initio</i> [15] | 5.8 | -6.9 | 2.4 | 1.8 | -5.9 | 3.2 |
| | <i>ab initio</i> [19] | 7.7 | -8.6 | 3.3 | 1.5 | -6.4 | 4.9 |
| | Shell model [28] | 8.2 | -8.6 | 3.0 | 1.2 | -6.4 | 4.0 |
| | LEED expt. [5] | 4.1±2 | -5±1 | 2±1 | 2.1±2 | 1±1 | -1±1 |
| | RHEED expt. [6] | 4.1 | 2.6 | 1.3 | 2.6 | 1.8 | 1.3 |
| | MEIS expt. [7] | | | | 1.5±0.2 | 0.5±0.2 | |
| BTO | This study | 1.3±12.1 | -0.3±3.6 | -6.7±2.8 | 12.8±8.5 | 0.3±1 | |
| | | | | | | | |
| | | 1.37 | -3.74 | 1.74 | 2.73 | -5.59 | 2.51 |
| | | (1.40) | (-3.79) | (1.70) | (2.69) | (-5.57) | 2.54 |
| | <i>ab initio</i> [14] | 1.39 | -3.71 | 0.39 | 2.26 | -5.2 | 2.06 |
| PTO | Shell model [20] | 0.37 | -2.42 | 2.39 | 1.4 | -6.5 | 3.17 |
| | Shell model [28] | 4.72 | -4.97 | 1.76 | 1.78 | -4.91 | 2.52 |
| PTO | This study | 3.51 | -6.89 | 3.07 | 3.12 | -8.13 | 5.32 |
| | | (3.78) | (-7.03) | (3.01) | (3.58) | (-8.28) | (5.44) |
| | <i>ab initio</i> [16] | 3.9 | -6.75 | 3.76 | 3.06 | -7.93 | 5.45 |

methods, which give the same sign for both the rumpling and change of interlayer distances. The amplitude of surface rumpling of SrO-terminated STO is predicted much larger than that for TiO₂-terminated STO surface, whereas the rumpling of BTO TiO₂-terminated surface is predicted to exceed by a factor of two that for BaO-terminated surface. Lastly, PTO demonstrates practically equal rumpling for both terminations. From Table 2 one can see that all surfaces show the reduction of interlayer distance d_{12} and expansion of d_{23} . The calculated surface rumpling agrees quite well with LEED, RHEED and MEIS experiments [5, 6, 7] (which are available for STO surfaces only). Theory agrees semi-quantitatively also with the LEED results for the Δd_{12} and Δd_{23} . However, from Table 2 is well seen that LEED and RHEED experiments contradict each other in the sign of Δd_{12} for SrO-terminated surface and Δd_{23} of TiO₂-terminated surface. Another problem is that LEED, RHEED and MEIS experiments demonstrate that the topmost oxygen always move outwards the surfaces whereas all calculations predict for the TiO₂-terminated STO surface that oxygen goes *inwards*. Even more important is the contradiction between the three above-mentioned experiments and recent SXRD study [8] where oxygen atoms are predicted to move inwards for *both* surface terminations reaching rumpling up to 12.8% for the TiO₂ terminated surface! Up to now the reason for such discrepancies between the different experimental data is not clear (see [8, 15]). Thus, the disagree-

Table 3: Calculated surface energies (in eV per surface cell). Results for previous *ab initio* calculations [16, 19, 21] are averaged over AO- and TiO₂-terminated surfaces.

| | STO | | | BTO | | | PTO | | |
|------------|------|------------------|--------|------|------------------|--------|------|------------------|--------|
| | SrO | TiO ₂ | asymm. | BaO | TiO ₂ | asymm. | PbO | TiO ₂ | asymm. |
| This study | 1.15 | 1.23 | 1.19 | 1.19 | 1.07 | 1.13 | 0.83 | 0.74 | 0.85 |
| [27] | 1.18 | 1.22 | | | | | | | |
| [28] | 1.32 | 1.36 | | 1.45 | 1.40 | | | | |
| [19] | | 1.21 | 1.19 | | | | | | |
| [21] | | | | | 1.17 | | | | |
| [16] | | 1.26 | | | 1.24 | | | 0.97 | |

ment between data obtained theoretically and experimentally cannot be analyzed until the conflict between different experimental results is resolved.

The calculated surface energies of the relaxed surfaces, presented in Table 3, were computed using the method described in Ref. [29]. One can see good agreement of the surface energies obtained by different methods. The energies calculated for AO- and TiO₂-terminated surfaces demonstrate a small difference, that means both terminations could co-exist. Nevertheless, the energy computed for TiO₂-terminated STO surface is a little bit larger than that for SrO-termination, in contrast to BTO and PTO crystals where TiO₂-terminated surface is a little bit energetically more favorable. The three (001) surfaces of A^{II}B^{IV}O₃ perovskites correspond to “type I” stable surfaces revealing the *weak-polarity* due to partly covalent nature of perovskite chemical bonding discussed in the next section.

3.2 Electronic Charge Redistribution

We begin discussion of the electronic structure of surfaces with the analysis of charge redistribution in near-surface planes. The effective atomic charges (calculated using the standard Mulliken population analysis) and dipole atomic moments characterizing atomic deformation along the *Z* axis are presented for all AO-, TiO₂- and asymmetrically terminated surfaces in Tables 4, 5, and 6, respectively. The differences in charge densities in the (001) planes in ABO₃ bulk crystals and on the (001) surfaces are analyzed in Table 7.

First of all, note that the effective charges of Sr and Ba are close to the +2e formal charges, whereas that of Pb is considerably smaller ($\sim 2e$). Ti and O charges are also much smaller than formal charges, similarly to the bulk [26] which results from the Ti-O covalent bonding. The AO-terminated surfaces of STO and BTO show similar behavior. The charges of top layer cations are smaller with respect to the relevant bulk charges, the oxygens attract an additional electron charge and

Table 4: The calculated Mulliken effective charges and dipole moments for the AO termination. Numbers in brackets are deviations from bulk values. Bulk charges (in e); STO: Sr = 1.871, Ti = 2.35, O = -1.407, BTO: Ba = 1.795, Ti = 2.364, O = -1.386, PTO: Pb = 1.343, Ti = 2.335, O = -1.226 [26].

| N | Ion | STO | | BTO | | PTO | |
|---|----------------|--------------------|--------------|--------------------|--------------|--------------------|--------------|
| | | Q, e | d, e a.u. | Q, e | d, e a.u. | Q, e | d, e a.u. |
| 1 | A | 1.845 (-0.026) | -0.2202 | 1.751 (-0.044) | -0.4634 | 1.277 (-0.066) | -0.4804 |
| | O | -1.524 (-0.117) | -0.0336 | -1.473 (-0.087) | -0.0532 | -1.131 (+0.095) | 0.0248 |
| 2 | Ti | 2.363 (+0.013) | 0.0106 | 2.377 (+0.013) | 0.0070 | 2.333 (-0.002) | -0.0211 |
| | O ₂ | -1.449 (-0.042) | -0.0191 | -1.417 (-0.031) | 0.0182 | -1.257 (-0.031) | -0.0062 |
| 3 | A | 1.875 (+0.004) | -0.0232 | 1.801 (+0.006) | -0.0433 | 1.354 (+0.011) | -0.0484 |
| | O | -1.429 (-0.022) | 0.0008 | -1.415 (-0.029) | -0.0084 | -1.258 (-0.032) | -0.0155 |
| 4 | Ti | 2.336 (-0.014) | 0 | 2.386 (+0.004) | 0 | 2.342 (+0.007) | 0 |
| | O ₂ | -1.411 (-0.004) | 0 | -1.392 (-0.006) | 0 | -1.232 (-0.006) | 0 |

Table 5: For the TiO₂ termination. The same as Table 4

| N | Ion | STO | | BTO | | PTO | |
|---|----------------|--------------------|--------------|--------------------|--------------|--------------------|--------------|
| | | Q, e | d, e a.u. | Q, e | d, e a.u. | Q, e | d, e a.u. |
| 1 | Ti | 2.314 (-0.036) | 0.0801 | 2.304 (-0.060) | 0.0816 | 2.279 (-0.056) | 0.0962 |
| | O ₂ | -1.324 (+0.083) | 0.0418 | -1.278 (+0.108) | 0.0207 | -1.182 (+0.044) | -0.0307 |
| 2 | A | 1.851 (-0.020) | 0.0423 | 1.765 (-0.030) | 0.0949 | 1.270 (-0.073) | 0.0990 |
| | O | -1.361 (+0.046) | -0.0436 | -1.343 (+0.043) | -0.0303 | -1.166 (+0.060) | -0.0060 |
| 3 | Ti | 2.386 (+0.036) | 0.0139 | 2.362 (-0.002) | 0.0079 | 2.332 (-0.003) | 0.0183 |
| | O ₂ | -1.389 (+0.018) | -0.0167 | -1.369 (+0.017) | -0.0108 | -1.205 (+0.021) | -0.0169 |
| 4 | A | 1.871 (0.000) | 0 | 1.794 (-0.001) | 0 | 1.337 (-0.006) | 0 |
| | O | -1.399 (+0.008) | 0 | -1.381 (+0.005) | 0 | -1.219 (+0.007) | 0 |

Table 6: For the asymmetrical termination. The same as Table 4

| N | Ion | STO | | BTO | | PTO | |
|----|----------------|----------|--------------|----------|--------------|----------|--------------|
| | | Q, e | d, e a.u. | Q, e | d, e a.u. | Q, e | d, e a.u. |
| 1 | A | 1.845 | -0.2238 | 1.751 | -0.4653 | 1.249 | -0.3055 |
| | | (-0.026) | | (-0.044) | | (-0.094) | |
| | O | -1.520 | -0.0428 | -1.470 | -0.0548 | -1.124 | 0.0305 |
| 2 | Ti | (-0.113) | | (-0.084) | | (+0.102) | |
| | | 2.361 | 0.0117 | 2.376 | 0.0054 | 2.318 | -0.0350 |
| | O ₂ | (+0.011) | | (+0.012) | | (-0.017) | |
| 3 | A | -1.450 | -0.0156 | -1.417 | 0.0265 | -1.242 | -0.0493 |
| | | (-0.043) | | (-0.031) | | (-0.016) | |
| | O | 1.874 | -0.0225 | 1.800 | -0.0461 | 1.345 | 0.0660 |
| 4 | Ti | (+0.003) | | (+0.005) | | (+0.002) | |
| | | -1.425 | 0.0067 | -1.414 | -0.0082 | -1.252 | 0.0062 |
| | O ₂ | (-0.018) | | (-0.028) | | (-0.026) | |
| 5 | A | 2.352 | 0.0026 | 2.366 | 0.0006 | 2.325 | 0.0025 |
| | | (+0.002) | | (+0.002) | | (-0.010) | |
| | O | -1.408 | -0.0006 | -1.389 | -0.0024 | -1.223 | -0.0323 |
| 6 | Ti | (-0.001) | | (-0.003) | | (+0.003) | |
| | | 1.870 | -0.0042 | 1.795 | -0.0074 | 1.334 | 0.1315 |
| | O | (-0.001) | | (0.000) | | (-0.009) | |
| 7 | A | -1.404 | 0.0102 | -1.384 | 0.0089 | -1.222 | 0.0425 |
| | | (+0.003) | | (+0.002) | | (+0.004) | |
| | O ₂ | 2.348 | -0.0089 | 2.362 | -0.0084 | 2.325 | -0.0115 |
| 8 | Ti | (-0.002) | | (-0.002) | | (-0.010) | |
| | | -1.383 | 0.0057 | -1.370 | 0.0103 | -1.200 | 0.0042 |
| | O | (+0.024) | | (+0.016) | | (+0.026) | |
| 9 | A | 1.846 | -0.0633 | 1.765 | -0.0950 | 1.260 | 0.0019 |
| | | (-0.022) | | (-0.030) | | (-0.083) | |
| | O | -1.365 | 0.0288 | -1.343 | 0.0318 | -1.149 | 0.0254 |
| 10 | Ti | (+0.042) | | (+0.043) | | (+0.077) | |
| | | 2.291 | -0.0748 | 2.305 | -0.0823 | 2.272 | -0.1508 |
| | O ₂ | (-0.059) | | (-0.059) | | (-0.063) | |
| 11 | A | -1.297 | -0.0493 | -1.278 | -0.0189 | -1.176 | -0.0048 |
| | | (+0.110) | | (+0.108) | | (+0.050) | |
| | O ₂ | | | | | | |

Table 7: Calculated charge densities in the (001) planes in the bulk perovskites (in e, per TiO_2 or AO unit, data are taken from [26]) and in four top planes of the AO-, TiO_2 -terminated and asymmetrical slabs. Deviations of charge density with respect to the bulk are given in brackets.

| Termination | N | Unit | STO | BTO | PTO |
|----------------|---|----------------|----------|----------|----------|
| Bulk | | AO | 0.464 | 0.409 | 0.117 |
| | | TiO_2 | -0.464 | -0.409 | -0.117 |
| AO | 1 | AO | 0.321 | 0.278 | 0.146 |
| | | | (-0.143) | (-0.131) | (0.029) |
| | 2 | TiO_2 | -0.535 | -0.457 | -0.181 |
| | | | (-0.071) | (-0.049) | (-0.064) |
| | 3 | AO | 0.446 | 0.386 | 0.096 |
| | | | (-0.018) | (-0.023) | (-0.021) |
| | 4 | TiO_2 | -0.486 | -0.398 | -0.122 |
| | | | (-0.022) | (0.010) | (-0.005) |
| TiO_2 | 1 | TiO_2 | -0.334 | -0.252 | -0.085 |
| | | | (0.130) | (0.156) | (0.032) |
| | 2 | AO | 0.490 | 0.422 | 0.104 |
| | | | (0.026) | (0.013) | (-0.013) |
| | 3 | TiO_2 | -0.392 | -0.376 | -0.078 |
| | | | (0.072) | (0.032) | (0.039) |
| | 4 | AO | 0.472 | 0.413 | 0.118 |
| | | | (0.008) | (0.004) | (0.001) |
| Asymmetrical | 1 | AO | 0.325 | 0.281 | 0.125 |
| | | | (-0.139) | (-0.128) | (0.008) |
| | 2 | TiO_2 | -0.539 | -0.458 | -0.166 |
| | | | (-0.075) | (-0.050) | (-0.049) |
| | 3 | AO | 0.449 | 0.386 | 0.093 |
| | | | (-0.015) | (-0.023) | (-0.024) |
| | 4 | TiO_2 | -0.464 | -0.421 | -0.121 |
| | | | (0.000) | (-0.004) | (-0.004) |
| | 5 | AO | 0.466 | 0.411 | 0.112 |
| | | | (0.002) | (0.002) | (-0.005) |
| | 6 | TiO_2 | -0.418 | -0.378 | -0.075 |
| | | | (0.046) | (0.030) | (0.042) |
| | 7 | AO | 0.481 | 0.422 | 0.111 |
| | | | (0.017) | (0.013) | (-0.006) |
| | 8 | TiO_2 | -0.303 | -0.251 | -0.080 |
| | | | (0.161) | (0.157) | (0.037) |

become more negative. The titanium ions in the second layer demonstrate the slight increase of their charges, their oxygens again became more negative due to addition electron charge transfer. Changes in atomic charges in deeper layers become very small and practically equal zero in the center of the slabs. Unlike STO and BTO, the surface oxygen on PbO-terminated surface becomes more positive, Ti in the second layer shows practically no changes in the effective charges.

The charge redistribution in the TiO_2 -terminated surfaces (Table 5) of all three perovskites demonstrates quite similar behavior. All cations in both topmost layers demonstrate charge reduction. For surface Ti it is a little bit larger then for A ions in subsurface layer. Changes of charges for ions in the asymmetrically terminated slabs (Table 6) are practically the same as for the symmetrically terminated AO- and TiO_2 - slab as it should be when slabs are thick enough and the two surfaces do not interact.

The calculated effective charges of ions in partly-covalent materials usually are far from the formal ionic charges due to electron density redistribution caused by the covalency effect, what is confirmed by our calculations (see also heading to Table 4). As a result, the AO and TiO_2 (001) planes in the bulk perovskites turn out to be *charged* with charge density per unit cell: $\sigma_B(\text{AO}) = -\sigma_B(\text{TiO}_2)$ (B means “Bulk”, Table 7). A half of this charge density comes from TiO_2 planes to each of the two neighboring AO planes. If the formal ionic charges (+4e, -2e, +2e) took place, the charge densities of the (001) planes would be zero and we deal with the neutral, “type-I surfaces” (according to the generally-accepted classification by Tasker [47]). In reality, the charge redistribution makes the $\text{ABO}_3(001)$ surfaces to be polar with the dipole moment perpendicular to the surface or “type-III polar surfaces”, which are potentially unstable. In case of symmetrically terminated slabs this dipole moment disappears due to symmetry, but the case of asymmetrical slabs is quite of interest. One of possibilities to stabilize the surface is to create surface defects [27]. Another option is to add the compensating charge density to the topmost layers of surfaces. The charge density changes for all perovskite surfaces with respect to the bulk magnitudes are summarized in Table 7. It is well seen, as a result of self-consistent calculations, the additional charge densities indeed exist, these are localized mainly on two upper layers whereas the central layers practically retain the bulk charge density. Such the electron charge density redistribution accompanied by atomic displacements on the surfaces allows to compensate the surface dipole moment even for the asymmetrically terminated slabs. Indeed, as one can see, the sum of changes in charge densities for three topmost layers of the asymmetrically terminated slab (on both sides) of all three perovskites approximately equals half the charge density of the corresponding bulk plane, which is necessary condition to

Table 8: The bond populations for the AO termination (in me, m=milli). Negative bond population means atomic repulsion. The corresponding bond populations for the bulk perovskites: Ti-O bond: (STO) 88; (BTO) 100; (PTO) 98; Pb-O bond: 16.

| Atom A | STO | | BTO | | PTO | |
|--------|--------|-----|--------|-----|--------|-----|
| | Atom B | | Atom B | | Atom B | |
| O(1) | O(1) | 4 | O(1) | 2 | O(1) | 0 |
| | Sr(1) | -6 | Ba(1) | -30 | Pb(1) | 54 |
| | Ti(2) | 72 | Ti(2) | 80 | Ti(2) | 102 |
| | O(2) | -54 | O(2) | -58 | O(2) | -74 |
| O(2) | Sr(1) | -30 | Ba(1) | -56 | Pb(1) | 52 |
| | O(2) | -46 | O(2) | -38 | O(2) | -60 |
| | Ti(2) | 78 | Ti(2) | 88 | Ti(2) | 80 |
| | Sr(3) | -10 | Ba(3) | -30 | Pb(3) | 6 |
| O(3) | O(3) | -48 | O(3) | -34 | O(3) | -42 |
| | Ti(2) | 86 | Ti(2) | 90 | Ti(2) | 72 |
| | O(3) | -8 | O(3) | -6 | O(3) | -8 |
| | Sr(3) | -12 | Ba(3) | -36 | Pb(3) | 24 |
| O(4) | Ti(4) | 84 | Ti(4) | 98 | Ti(4) | 96 |
| | O(4) | -46 | O(4) | -38 | O(4) | -54 |
| | Sr(3) | -10 | Ba(3) | -34 | Pb(3) | 24 |
| | O(4) | -8 | O(4) | -6 | O(4) | -8 |
| | Ti(4) | 86 | Ti(4) | 98 | Ti(4) | 94 |

remove the macroscopic dipole moment [47]. These results are in a line with ideas of “weak polarity” [2, 48].

The atomic *dipole moments* characterize the deformation and polarization along the z -axis perpendicular to the surface [32]. These are presented in Tables 4, 5, 6 for AO-, TiO₂- and asymmetrically terminated surfaces, respectively. On the AO-terminated surfaces of all three perovskites the cations have the negative dipole moments, directed inwards, to the slab center. The dipole moments of surface Sr, Ba and Pb cations on AO-terminated surfaces are surprisingly large, several times larger than those of other ions, including the TiO₂-terminated surfaces. Oxygens of the AO-terminated surfaces of STO and BTO demonstrate small negative dipole moments whereas for the PTO the oxygen dipole moment is positive. The polarization of second and third layers is pretty small.

On the TiO₂ terminated surfaces polarization of cations has a positive sign, as well as for the oxygens in STO and BTO. In contrast, oxygens on PbO surface have negative dipole moment. Cations of subsurface layers for all three perovskites reveal the positive dipole moments whereas those of oxygens are negative. The asymmetrically terminated slabs, actually, reproduce the polarization picture obtained for the two relevant symmetrically terminated slabs.

The Mulliken *bond populations* between atoms in surface layers (which arise due to covalency) are presented for the AO-, TiO₂- and asymmetrically terminated

Table 9: The same as Table 8 for the TiO_2 termination.

| Atom A | STO | | BTO | | PTO | |
|--------|--------|-----|--------|-----|--------|-----|
| | Atom B | | Atom B | | Atom B | |
| O(1) | O(1) | -30 | O(1) | -24 | O(1) | -34 |
| | Ti(1) | 114 | Ti(1) | 126 | Ti(1) | 114 |
| | Sr(2) | -14 | Ba(2) | -38 | Pb(2) | 42 |
| | O(2) | -28 | O(2) | -20 | O(2) | -42 |
| O(2) | Ti(1) | 142 | Ti(1) | 140 | Ti(1) | 162 |
| | O(2) | 2 | O(2) | 2 | O(2) | 0 |
| | Sr(2) | -8 | Ba(2) | -30 | Pb(2) | 8 |
| | Ti(3) | 72 | Ti(3) | 90 | Ti(3) | 80 |
| O(3) | O(3) | -36 | O(3) | -32 | O(3) | -36 |
| | Sr(2) | -4 | Ba(2) | -24 | Pb(2) | 14 |
| | O(3) | -42 | O(3) | -36 | O(3) | -44 |
| | Ti(3) | 94 | Ti(3) | 106 | Ti(3) | 110 |
| O(4) | Sr(4) | -10 | Ba(4) | -34 | Pb(4) | 18 |
| | O(4) | -42 | O(4) | -36 | O(4) | -44 |
| | Ti(3) | 92 | Ti(3) | 102 | Ti(3) | 106 |
| | O(4) | 2 | O(4) | 2 | O(4) | 2 |
| | Sr(4) | -10 | Ba(4) | -34 | Pb(4) | 14 |

slabs in Tables 8, 9 and 10, respectively. The largest effect is observed for PTO crystal: the population of the Pb-O bond on the top layer increases a factor of three, as compared to the bulk. The partly covalent nature of Pb-O bond in lead titanate crystal due to hybridization of Pb 6s AO state with the O 2p AO is already pronounced in the bulk [26], but due to bond shortening (due to surface relaxation) its covalency is increased. This effect is also observed on the TiO_2 surface, for the bond population between surface O and Pb in the second plane. Unlike PTO, in STO and BTO there is no indication on the Sr-, Ba- bonding with O atoms. Unlike Pb, these cations have effective charges close to formal charge +2e (Table 4). The Ti-O bonds of all three perovskites on the TiO_2 terminated surfaces increase their covalency due to bond shortening (caused by surface relaxation) and breaking O surface bonds (Table 9). In line with Ref. [27, 28], we observe $\approx 50\%$ increase of the Ti-O bond covalency on the (001) surface. The asymmetrically terminated slabs demonstrate practically the same bond populations as discussed above AO- and TiO_2 -terminated slabs.

The *difference electron density maps* calculated with respect to the superposition density of spherical A^{2+} , Ti^{4+} and O^{2-} ions for STO, BTO and PTO surfaces are presented in Fig. 3, 4 and 5, respectively. These maps demonstrate considerable electron charge density redistribution near the perovskite surfaces and are entirely consistent with the above-discussed Mulliken charges and bond population analysis. For all three perovskites the excess of electron density (the solid isodensity curves) is

Table 10: The same as Table 8 for the asymmetrical termination.

| Atom A | STO | | BTO | | PTO | |
|--------|--------|-----|--------|-----|--------|-----|
| | Atom B | | Atom B | | Atom B | |
| O(1) | O(1) | 4 | O(1) | 2 | O(1) | 0 |
| | Sr(1) | -6 | Ba(1) | -30 | Pb(1) | 58 |
| | Ti(2) | 70 | Ti(2) | 82 | Ti(2) | 104 |
| O(2) | O(2) | -56 | O(2) | -60 | O(2) | -70 |
| | Sr(1) | -32 | Ba(1) | -58 | Pb(1) | 48 |
| | O(2) | -46 | O(2) | -38 | O(2) | -58 |
| | Ti(2) | 76 | Ti(2) | 88 | Ti(2) | 88 |
| | Sr(3) | -10 | Ba(3) | -30 | Pb(3) | 6 |
| O(3) | O(3) | -48 | O(3) | -32 | O(3) | -44 |
| | Ti(2) | 86 | Ti(2) | 90 | Ti(2) | 82 |
| | O(3) | 2 | O(3) | -6 | O(3) | 0 |
| | Sr(3) | -12 | Ba(3) | -36 | Pb(3) | 26 |
| | Ti(4) | 86 | Ti(4) | 98 | Ti(4) | 98 |
| O(4) | O(4) | -46 | O(4) | -38 | O(4) | -52 |
| | Sr(3) | -10 | Ba(3) | -34 | Pb(3) | 14 |
| | O(4) | -8 | O(4) | 2 | O(4) | -8 |
| | Ti(4) | 88 | Ti(4) | 98 | Ti(4) | 100 |
| | Sr(5) | -10 | Ba(5) | -34 | Pb(5) | 14 |
| O(5) | O(5) | -44 | O(5) | -38 | O(5) | -50 |
| | Ti(4) | 88 | Ti(4) | 102 | Ti(4) | 102 |
| | O(5) | 2 | O(5) | -6 | O(5) | 0 |
| | Sr(5) | -10 | Ba(5) | -34 | Pb(5) | 18 |
| | Ti(6) | 88 | Ti(6) | 102 | Ti(6) | 102 |
| O(6) | O(6) | -44 | O(6) | -36 | O(6) | -50 |
| | Sr(5) | -10 | Ba(5) | -34 | Pb(5) | 24 |
| | O(6) | -42 | O(6) | -36 | O(6) | -44 |
| | Ti(6) | 96 | Ti(6) | 104 | Ti(6) | 110 |
| | Sr(7) | -4 | Ba(7) | -24 | Pb(7) | 14 |
| O(7) | O(7) | -36 | O(7) | -32 | O(7) | -34 |
| | Ti(6) | 80 | Ti(6) | 90 | Ti(6) | 84 |
| | O(7) | 2 | O(7) | 2 | O(7) | 0 |
| | Sr(7) | -8 | Ba(7) | -30 | Pb(7) | 8 |
| | Ti(8) | 132 | Ti(8) | 142 | Ti(8) | 160 |
| O(8) | O(8) | -28 | O(8) | -20 | O(8) | -40 |
| | Sr(7) | -14 | Ba(7) | -38 | Pb(7) | 42 |
| | Ti(8) | 118 | Ti(8) | 126 | Ti(8) | 116 |
| | O(8) | -32 | O(8) | -24 | O(8) | -32 |

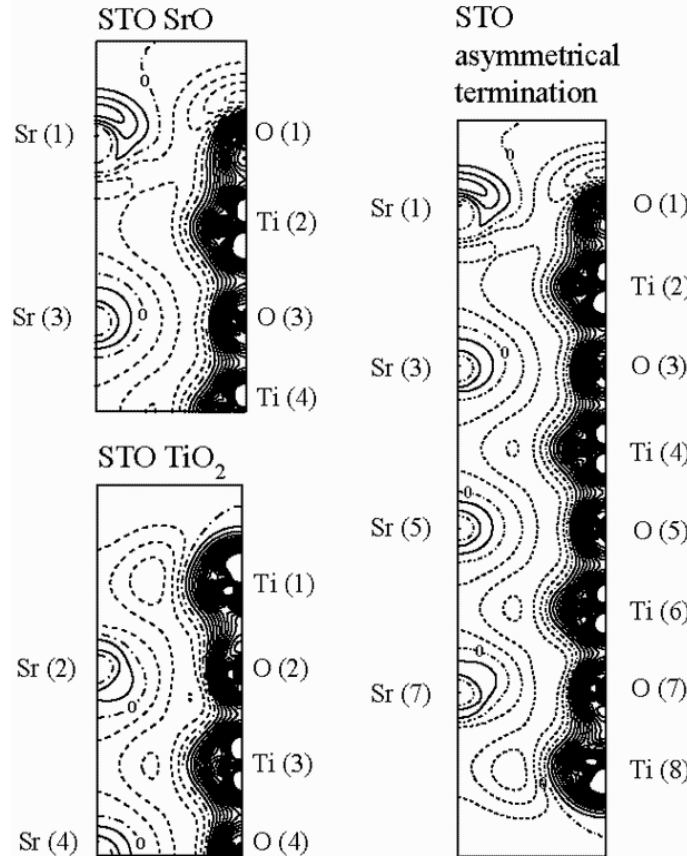


Figure 3: The difference electron density maps in the cross section perpendicular to the (001) surface ((110) plane) with the AO-, TiO₂ and asymmetrical terminations. Isodensity curves are drawn from -0.05 to +0.05 e a.u.⁻³ with an increment of 0.0025 e a.u.⁻³.

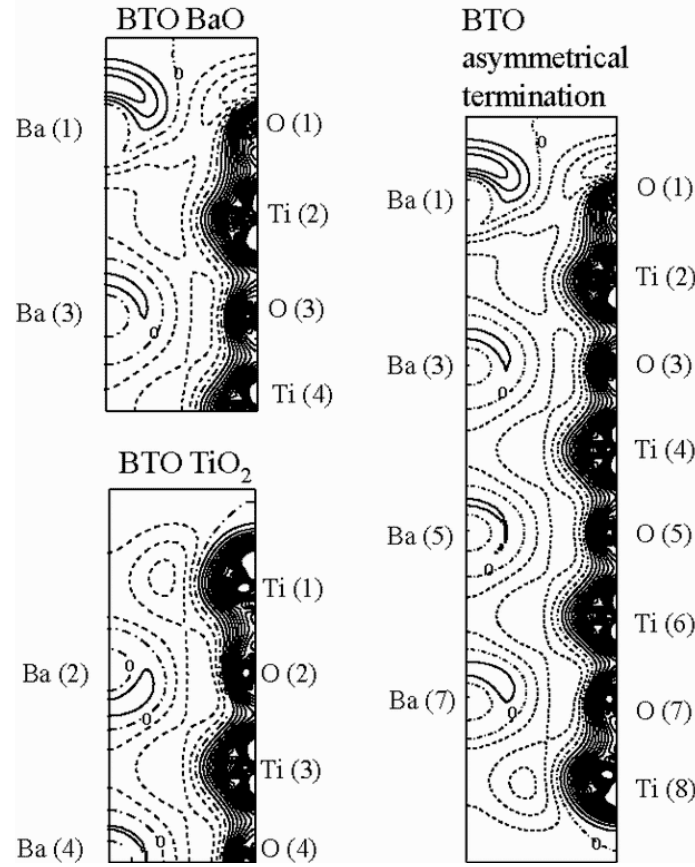


Figure 4: The BTO difference electron density maps. The same as Fig. 3.

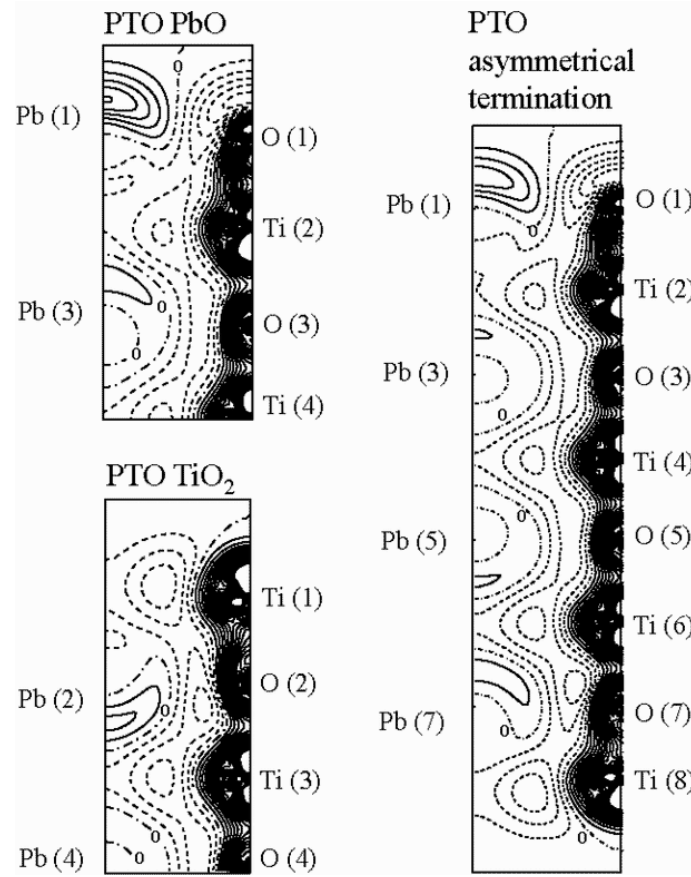


Figure 5: The PTO difference electron density maps. The same as Fig. 3.

observed for the Ti-O bonds, which corresponds to the bond covalency. For all terminations nearest to the surface Ti-O bond becomes stronger, but the next nearest bond becomes weaker. The A cations on the AO-terminated surfaces demonstrate considerable polarization, as it was predicted above from dipole moment calculations (Tables 4, 5 and 6). Nevertheless, the electron density maps demonstrate no clear trace of the covalent bonding (zero dot-dashed curves in area between A cations and Ti-O pairs) between A cations and oxygen, even for PTO, despite the Pb-O bond population (Table 8) was calculated as 54 me. This means, in reality the covalent contribution in Pb-O bond in PTO is quite weak and plays negligible role in the covalency of a whole PTO crystal. Note that the calculated Pb-O bond population considerably depends on the Mulliken population analysis and the Pb atomic BS [26], whose the most diffuse exponent (0.142 bohr^{-2}) mainly contributes into the increase of covalency. Indeed, recently suggested new approach for the population analysis using minimal valence basis of Wannier Type Atomic Orbitals (WTAO) [49] (which are directly connected to the electronic band structure) predicts practically ionic Pb charge $+1.99e$ for the bulk PTO crystal. Thus, our calculated Pb-O bond population can be interpreted as an increase of the electron attraction between Pb and O ions rather a real covalency.

3.3 Density of States and Band Structures

The calculated *band structures* for STO and BTO bulk and surfaces (Fig. 6 and 7) are quite similar. The band structure for the *bulk* perovskites was calculated using a unit cell which is fourfold extended along the z -axis. Such a supercell is similar to the eight-layer “slab” periodically repeated in 3D space and provides also the most natural comparison with the surface band structures. In the bulk band structure calculations the bands are plotted using the Γ -X-M- Γ directions of the typical “surface” Brillouin zone (which is simply a square in cubic crystals with the standard high symmetry points: Γ in the center, M the corner and X the center of square edge). The upper valence bands (VB) for the STO and BTO bulk are quite flat with the top in M point and perfectly flat fragment between M and X points. The main contribution into the upper VB comes from O $2p_x$ and $2p_y$ as it is well seen from the calculated density of states (DOS) projected onto the corresponding atomic orbitals (AOs) (see Fig. 9 and 12). The bottom of lowest conduction band (CB) lies at the Γ point with quite flat fragment between the Γ and X points and consist of Ti $3d$ threefold degenerated T_{2g} level. The optical band gaps for surfaces and bulk of all three perovskites as calculated by means of the DFT-B3PW are presented in Table 11. One can see a good agreement with experiment. We should

Table 11: The calculated optical gap (in eV) for the bulk [26] and surface-terminated perovskites. The numbers in brackets are from Ref. [27] for STO and Ref. [53] for PTO. Both these calculations had no d -orbitals on O, and the later one is done with B3LYP functional. The last row contains experimental data.

| | STO | | | | BTO | | | | PTO | | | |
|------------------------|---------------------|----------------|------------------|------|-----------|------|------------------|------|----------------|----------------|------------------|------|
| | bulk | SrO | TiO ₂ | asm | bulk | BaO | TiO ₂ | asm | bulk | PbO | TiO ₂ | asm |
| Direct gap | | | | | | | | | | | | |
| Γ - Γ | 3.96 (4.43) | 3.72 (4.12) | 3.95 (3.78) | 3.03 | 3.55 | 3.49 | 2.96 | 2.73 | 4.32 (4.43) | 3.58 (3.61) | 3.18 (3.77) | 3.08 |
| X-X | 4.53 (5.08) | 4.37 (4.70) | 4.04 (4.38) | 4.09 | 4.39 | 4.22 | 3.63 | 3.72 | 3.02 (3.21) | 3.79 (3.82) | 3.10 (3.12) | 3.28 |
| M-M | 5.70 (6.45) | 5.62 (5.94) | 5.17 (5.04) | 4.66 | 5.39 | 5.40 | 4.17 | 4.17 | 5.55 (5.80) | 5.37 (6.02) | 5.01 (4.89) | 4.88 |
| R-R | 6.47 (7.18) | | | | 6.12 | | | | 5.98 | | | |
| Indirect gap | | | | | | | | | | | | |
| X- Γ | 4.39 | 3.55 | 3.92 | 3.41 | 4.20 | 3.49 | 3.41 | 3.18 | 2.87 (3.18) | 2.96 (3.03) | 2.98 (3.12) | 2.78 |
| M- Γ | 3.71 (4.23) | 3.30 (3.71) | 3.17 (3.09) | 2.31 | 3.60 | 3.32 | 2.33 | 2.10 | 3.66 (3.85) | 3.55 (4.05) | 3.19 (2.99) | 2.96 |
| R- Γ | 3.63 (4.16) | | | | 3.50 | | | | 3.66 | | | |
| LDA-DFT PF (Ref. [16]) | | | | | | | | | | | | |
| | 1.85 | 1.86 | 1.13 | | 1.79 | 1.80 | 0.84 | | 1.54 | 1.53 | 1.61 | |
| Experiment | | | | | | | | | | | | |
| | 3.75 - direct gap | | | | 3.2 | | | | 3.4 | | | |
| | 3.25 - indirect gap | | | | Ref. [50] | | | | Ref. [51] | | | |
| | Ref. [52] | | | | | | | | | | | |

Table 12: The calculated positions of the valence band top ε_v and of the conduction band bottom ε_c (in eV) for relaxed and unrelaxed perovskite surface structures. The values in brackets are results from Ref. [53] for PTO. The conduction band bottom is in Γ -point. The valence band top lies at the M-point for STO and BTO, but in X-point for PTO. In the Ref. [53] the valence band top at the TiO₂-terminated surface is in M-point.

| | STO | | BTO | | PTO | |
|---------------------|-------|------------------|-------|------------------|---------------|------------------|
| | SrO | TiO ₂ | BaO | TiO ₂ | PbO | TiO ₂ |
| Unrelaxed structure | | | | | | |
| ε_c | 1.21 | -2.59 | 0.51 | -2.86 | -1.67 | -2.39 |
| ε_v | -2.48 | -5.22 | -3.01 | -5.39 | -4.59 | -5.14 |
| Relaxed structure | | | | | | |
| ε_c | -0.50 | -2.78 | 0.40 | -4.00 | -2.11 (-2.13) | -3.04 (-2.08) |
| ε_v | -3.80 | -5.95 | -2.92 | -6.33 | -5.07 (-5.16) | -6.02 (5.07) |

stress here remarkable agreement of the B3PW bulk gap with the experiment for STO (3.6 eV *vs* 3.3 eV). This is in a sharp contrast with the typical HF overestimate of the gap and DFT underestimate (*e.g.* 1.8 eV for STO, BTO [14, 15]).

The band structure for the SrO-terminated surface demonstrates practically the same flat the upper VB as in the bulk STO, with the top of VB at the M point and the bottom of CB at the Γ . The optical band gap for the SrO-terminated surface becomes smaller with respect to the band gap of the bulk STO. The narrow indirect gap between the Γ and M points is 3.3 eV, whereas the narrowest gap in the bulk is 3.63 eV, *i.e.* surface gap is reduced by 0.3 eV (see Table 11 for details). Analysis of the Density Of States (DOS) calculated for the SrO-terminated surface (Fig. 10) demonstrates no contribution of the surface O 2*p* states into the top of VB which mainly consists of 2*p* AOs of the oxygens from the *central* plane. The main contribution into the CB bottom comes from the Ti 3*d* which are in the second layer.

The band structure calculated for another, TiO₂-terminated surface of STO demonstrates less flatness of the VB top, in a comparison with the SrO-termination. The indirect optical band gap (M- Γ) 3.17 eV becomes by ≈ 0.46 eV narrower as compared with the bulk, *i.e.* twice more reduced as the SrO-terminated surface. For the TiO₂-terminated STO surface the main contribution into the top of VB is made by O 2*p_x* and 2*p_y* AOs which are perpendicular to Ti-O-Ti bridge (see Fig. 11). The main contribution to the CB bottom comes from the 3*d* AOs of Ti in third layer, the energy levels of surface Ti lie a little bit higher in the energy. The calculated STO DOS are in a good agreement with MIES and UPS spectra recently measured for the TiO₂-terminated STO(001) surface [10]. Moreover, our calculated position of the VB top for TiO₂-terminated STO with respect to the vacuum (5.9 eV) practically coincides with the experimentally observed value of 5.7 ± 0.2 eV (Ref. [10]).

The band structure calculated for the asymmetrically terminated slab demonstrates the mixture of band structures obtained for the two symmetrically terminated slabs discussed above. The STO band gap becomes narrower (2.31 eV). The VB top consists mainly of O 2*p* from TiO₂-terminated slab surface, and the CB bottom from 3*d* AOs of Ti from a subsurface layer (II in Fig. 1(c)). The split of the upper VB (≈ 0.8 eV) is well pronounced in asymmetrical STO slab. The band structure of the BTO(001) surfaces demonstrates practically the same behavior as STO does (Fig. 7, 12, 13, 14, and Table 11). Nevertheless, the split of the VB upper band is pronounced more for the TiO₂-terminated BTO, as compared with the STO surface. Due to hybridization of Pb 6*s* and O 2*p* orbitals in PTO, the calculated band structure and DOS slightly differ from those calculated for STO and BTO (Fig. 8,

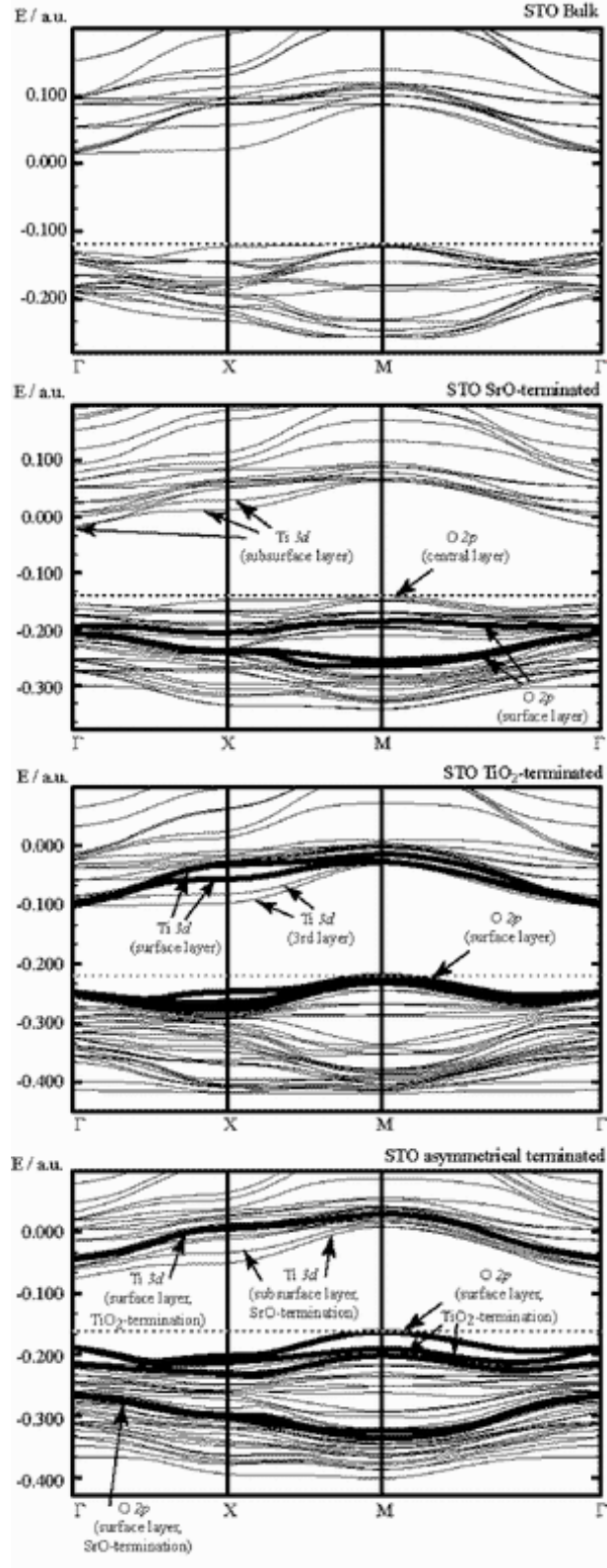


Figure 6: The calculated electronic band structure for STO bulk and surfaces.

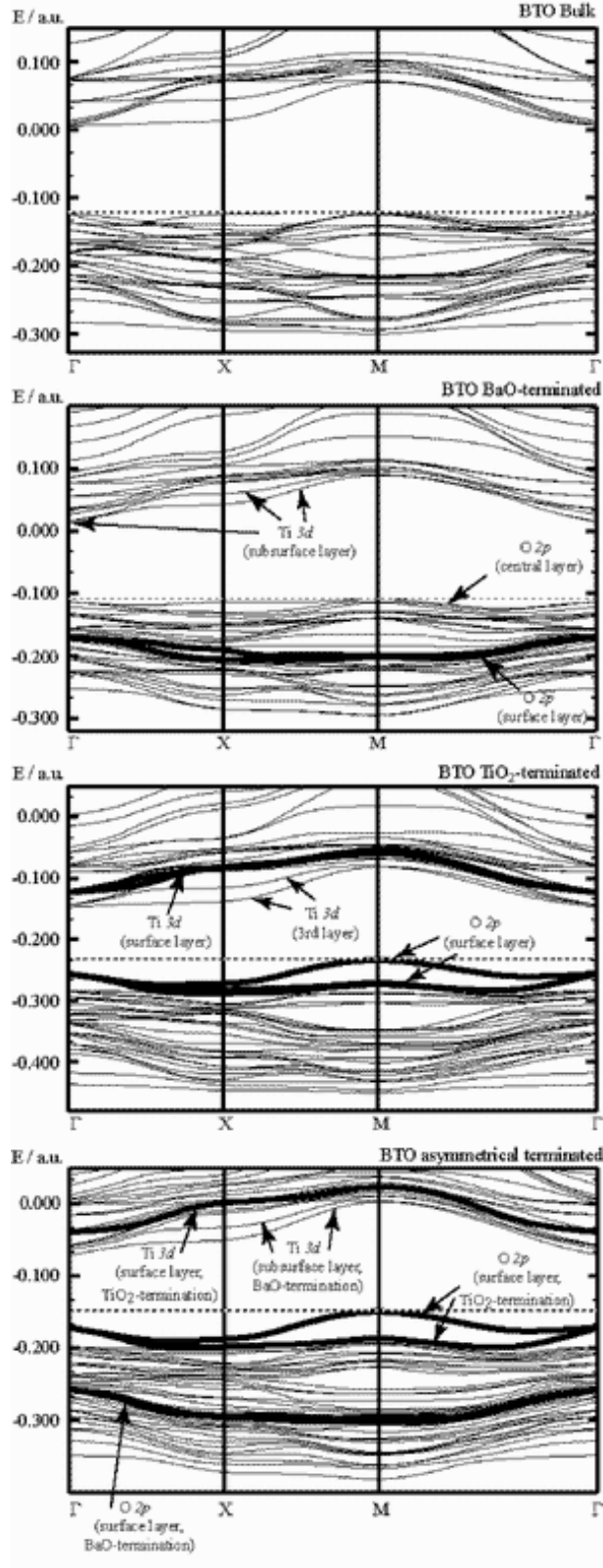


Figure 7: The calculated electronic band structure for BTO bulk and surfaces.

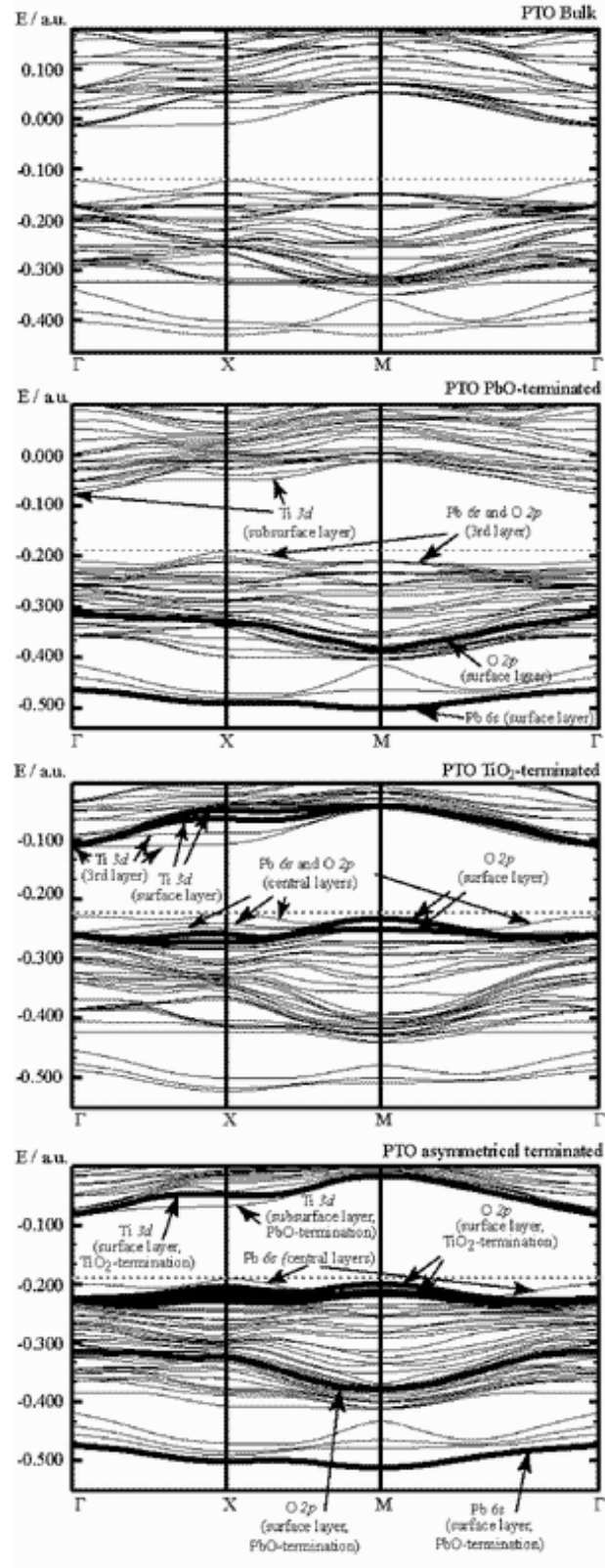


Figure 8: The calculated electronic band structure for PTO bulk and surfaces.

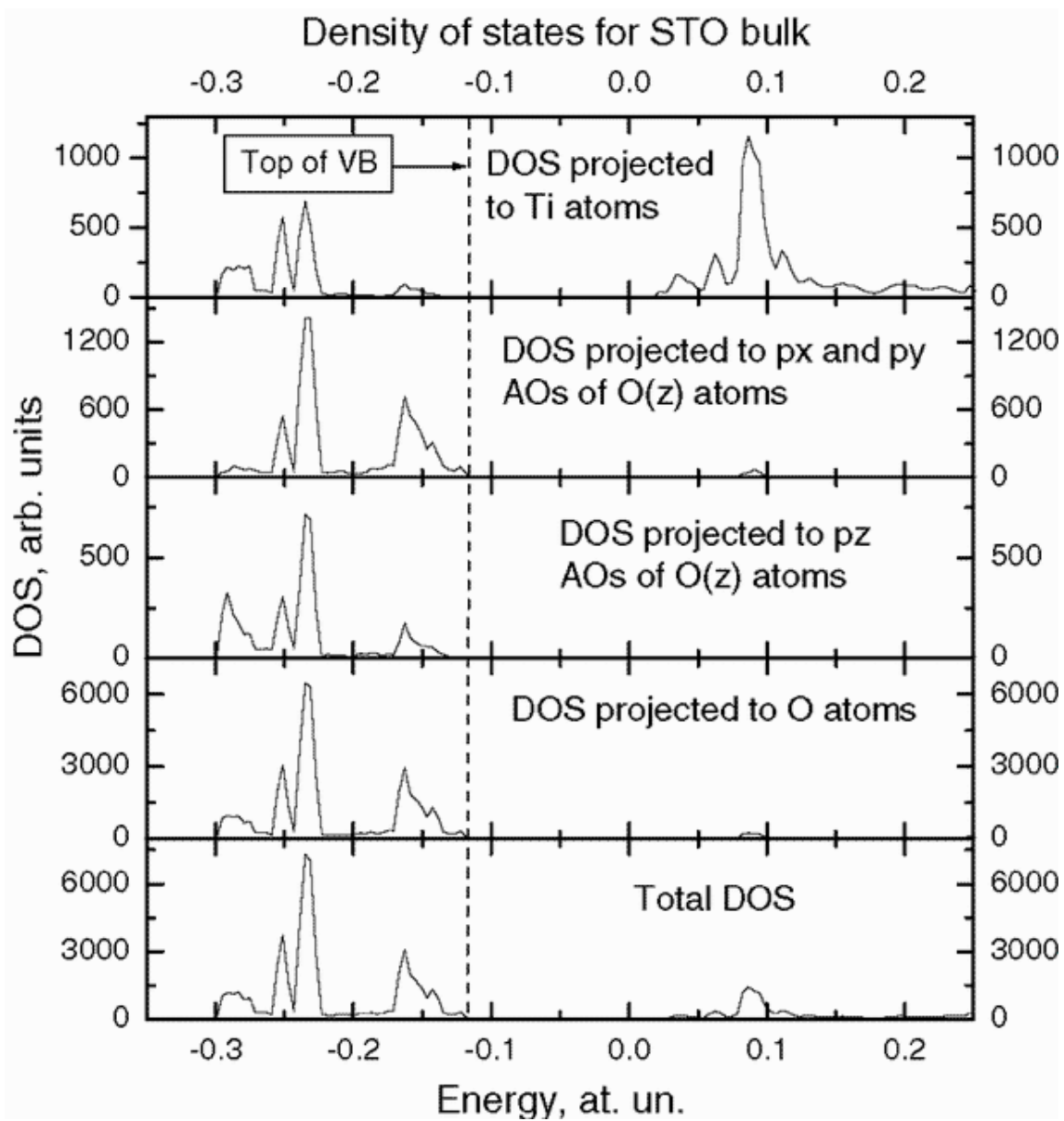


Figure 9: Total and projected DOS for the bulk STO.

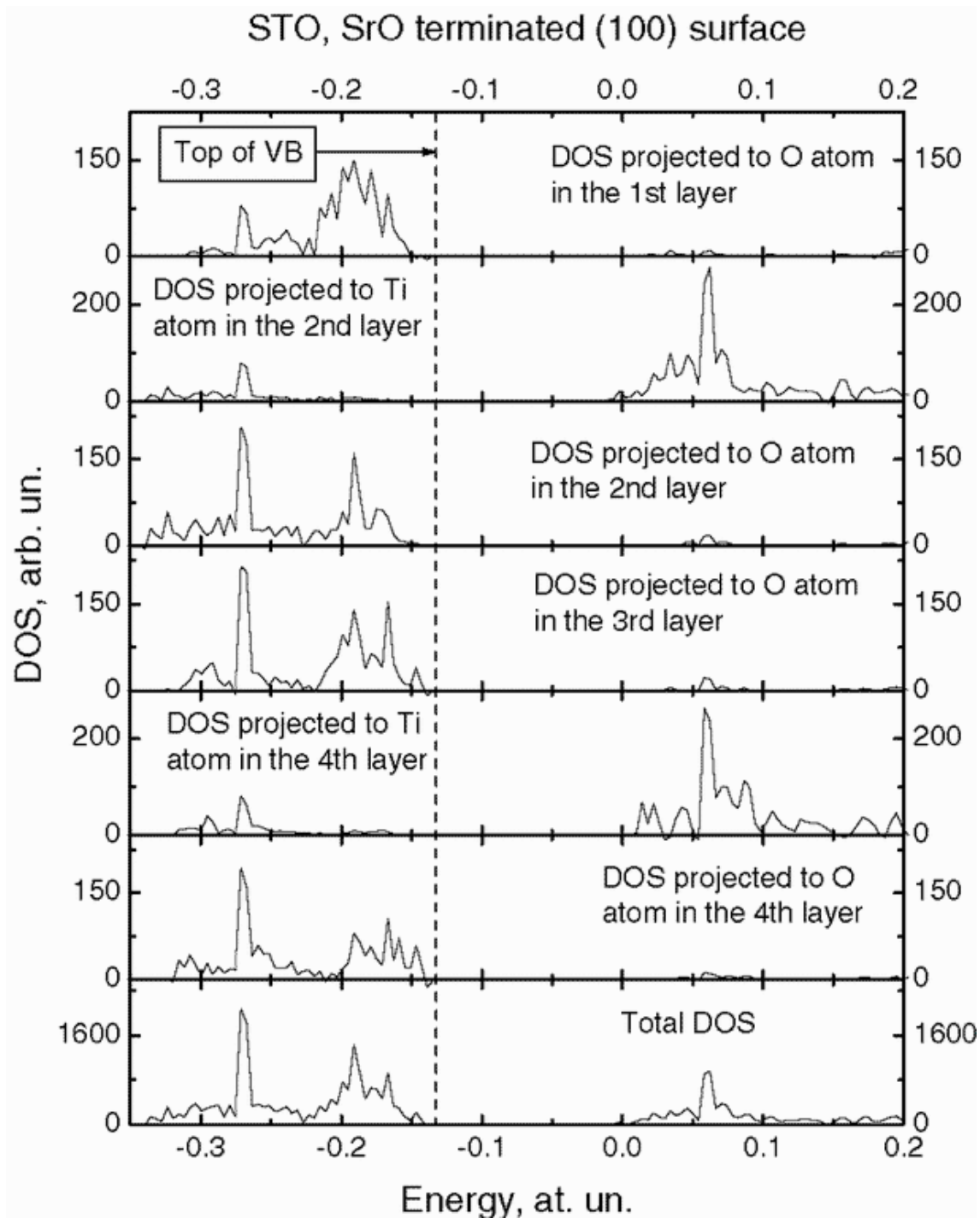


Figure 10: Total and projected DOS for the SrO-terminated surface.

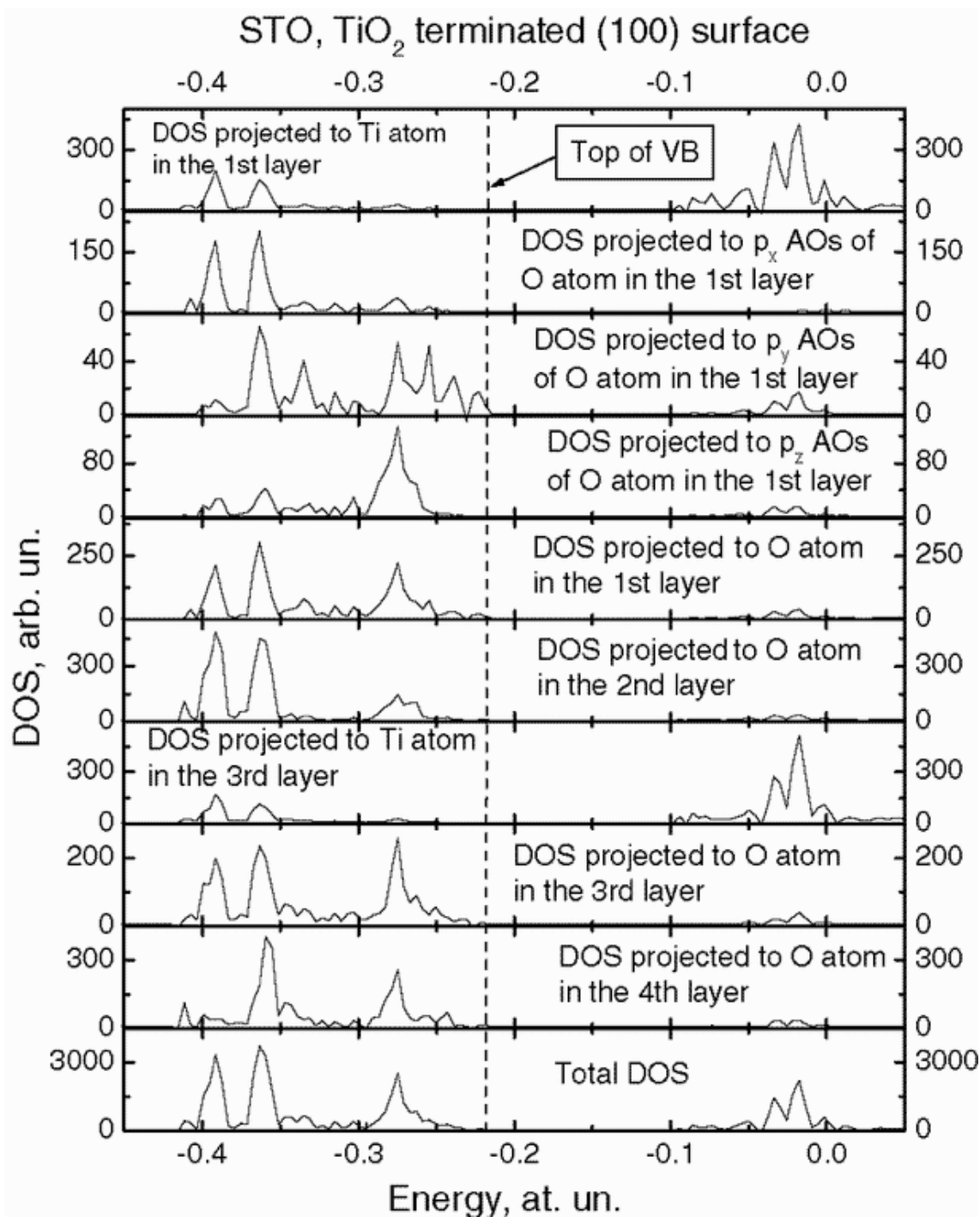


Figure 11: Total and projected DOS for the STO TiO_2 -terminated surface.

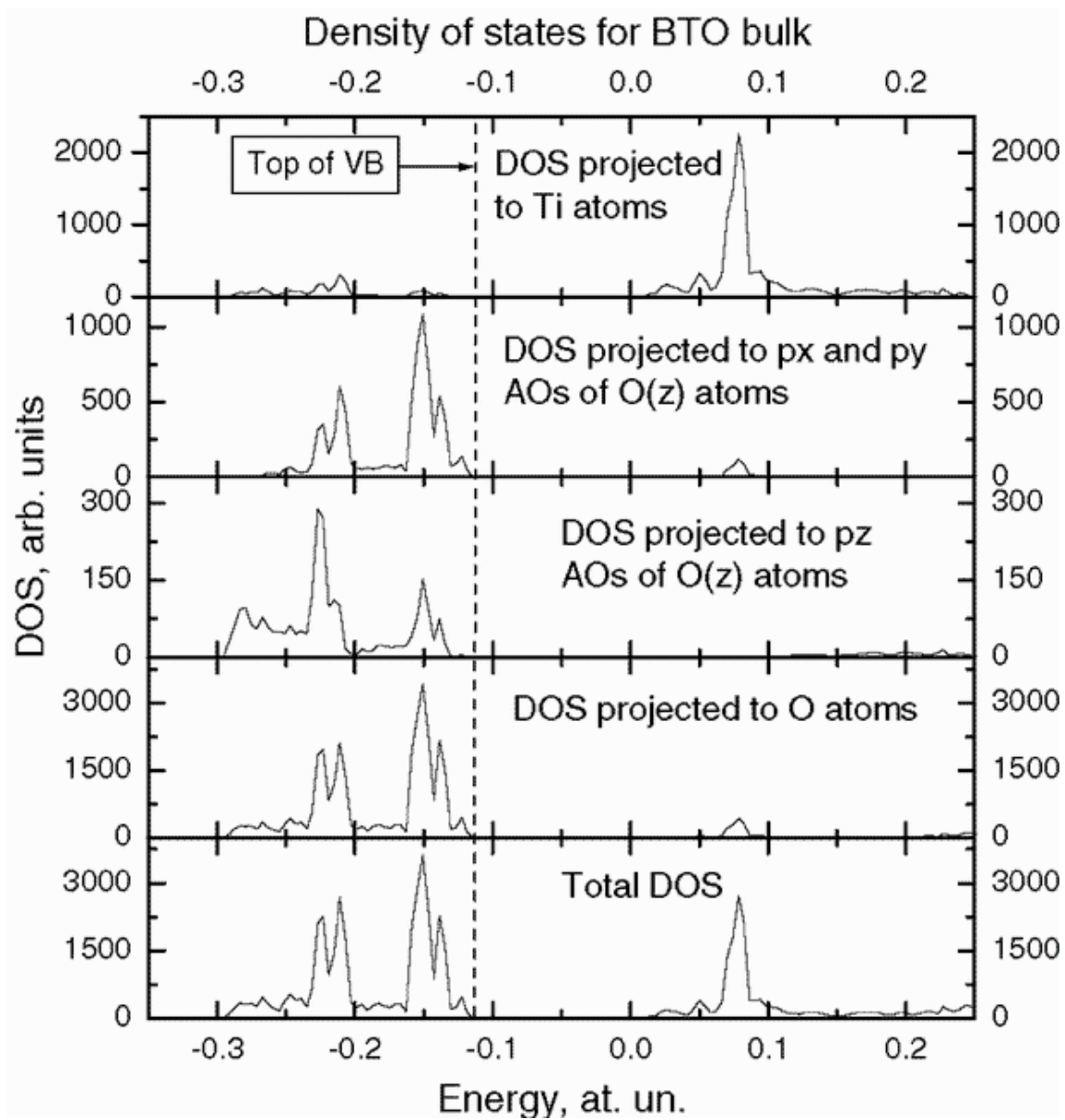


Figure 12: Total and projected DOS for the bulk BTO.

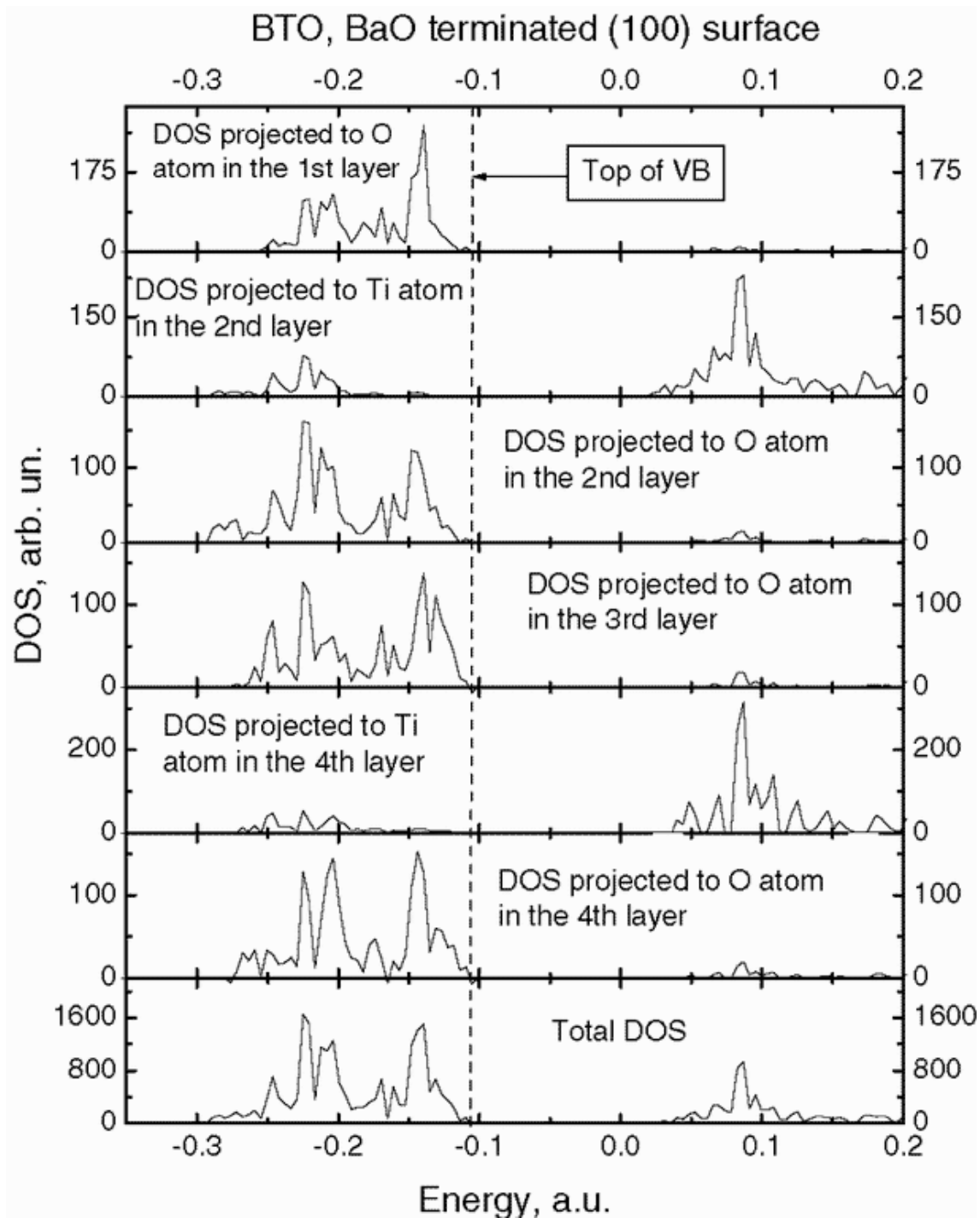


Figure 13: Total and projected DOS for the BaO-terminated surface.

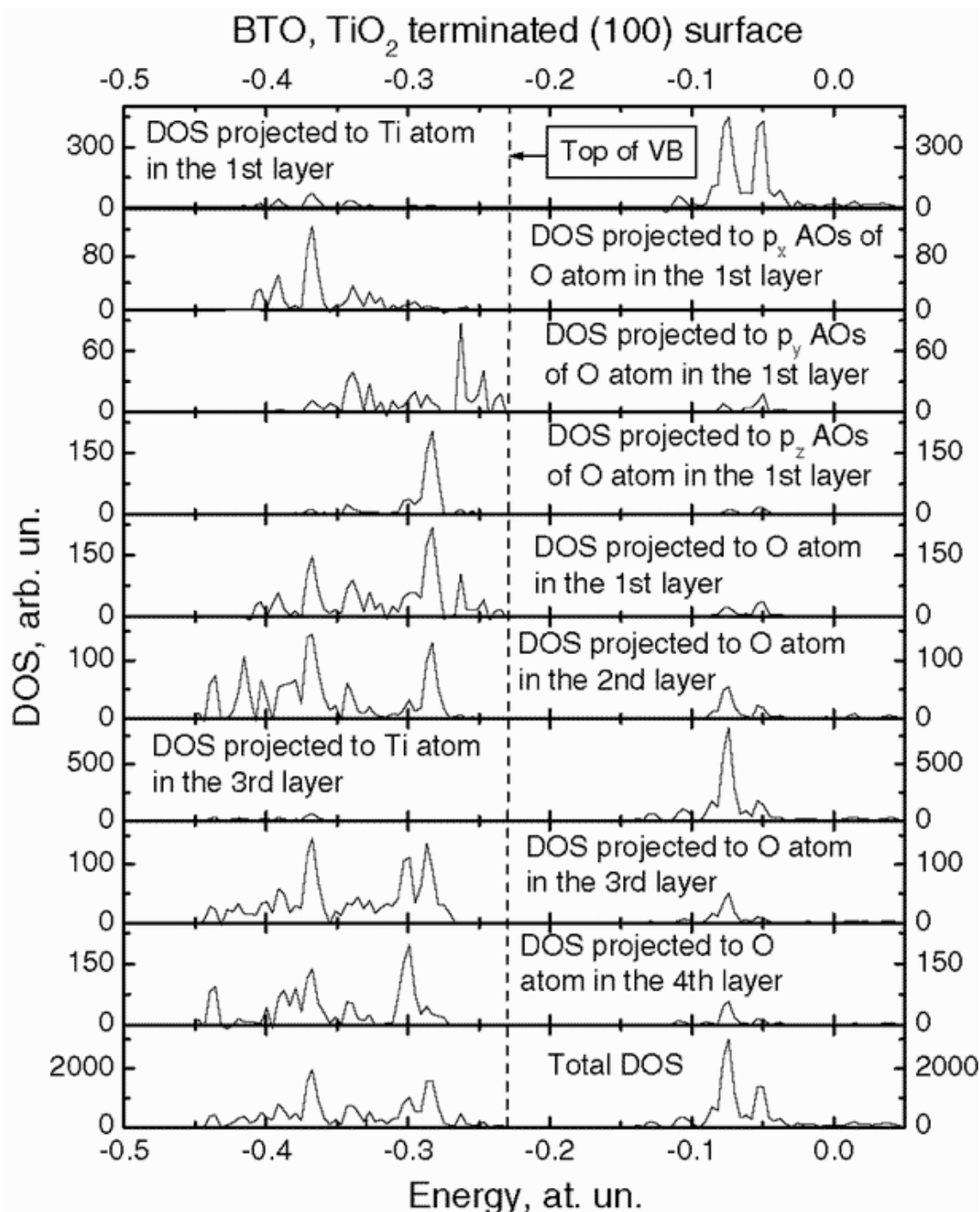


Figure 14: Total and projected DOS for the BTO TiO_2 -terminated surface.

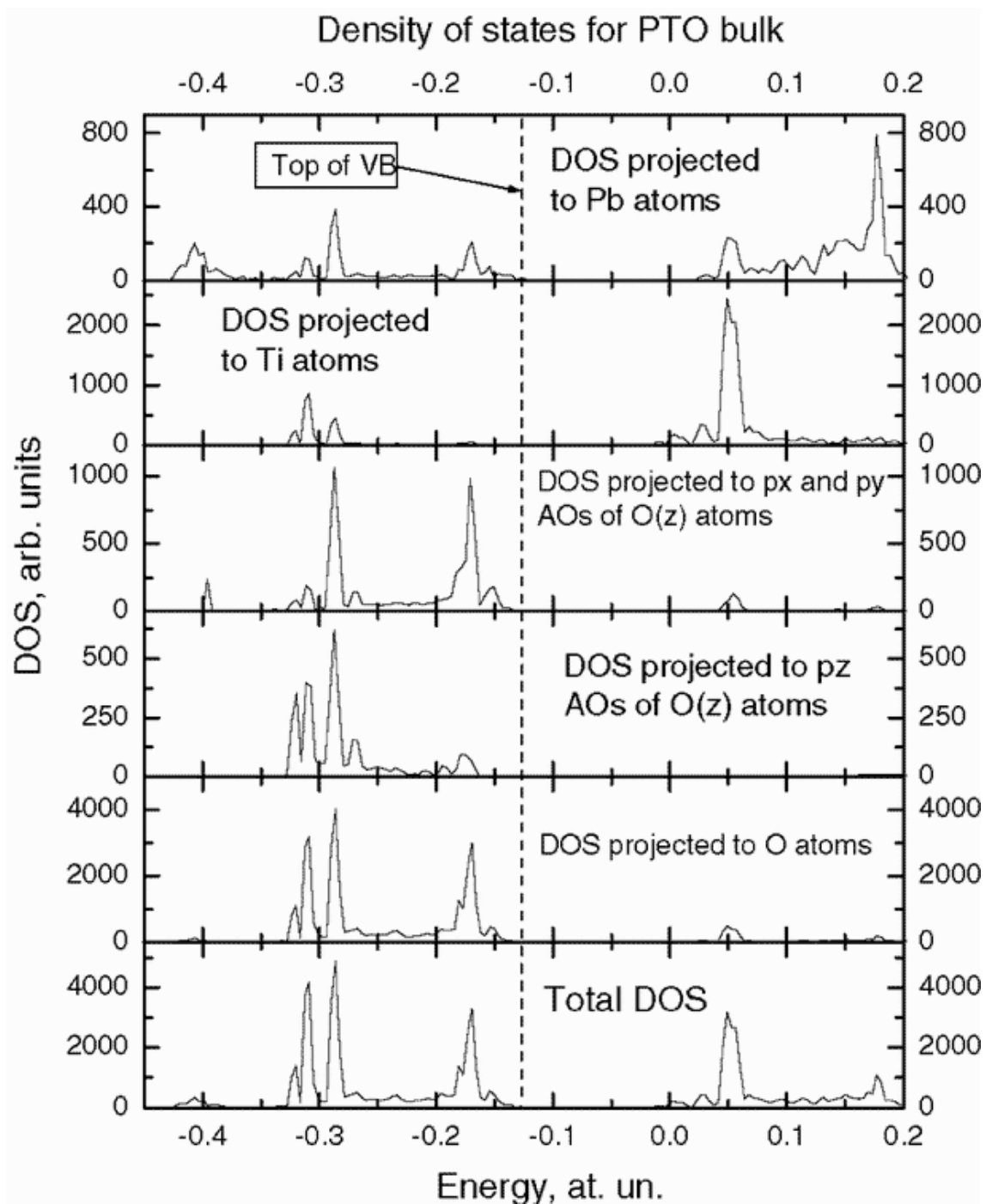


Figure 15: Total and projected DOS for the bulk PTO.

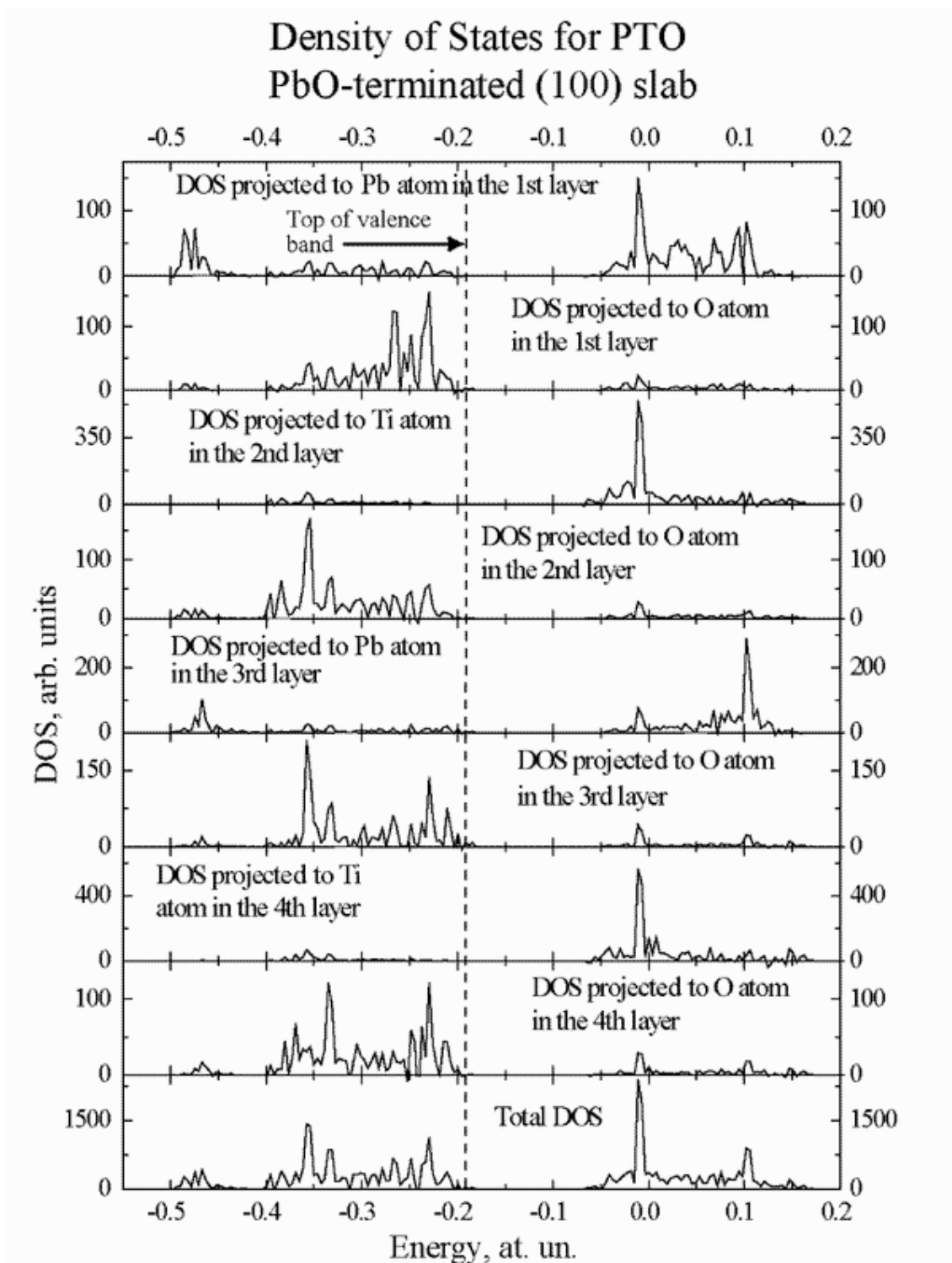


Figure 16: Total and projected DOS for the PbO-terminated surface.

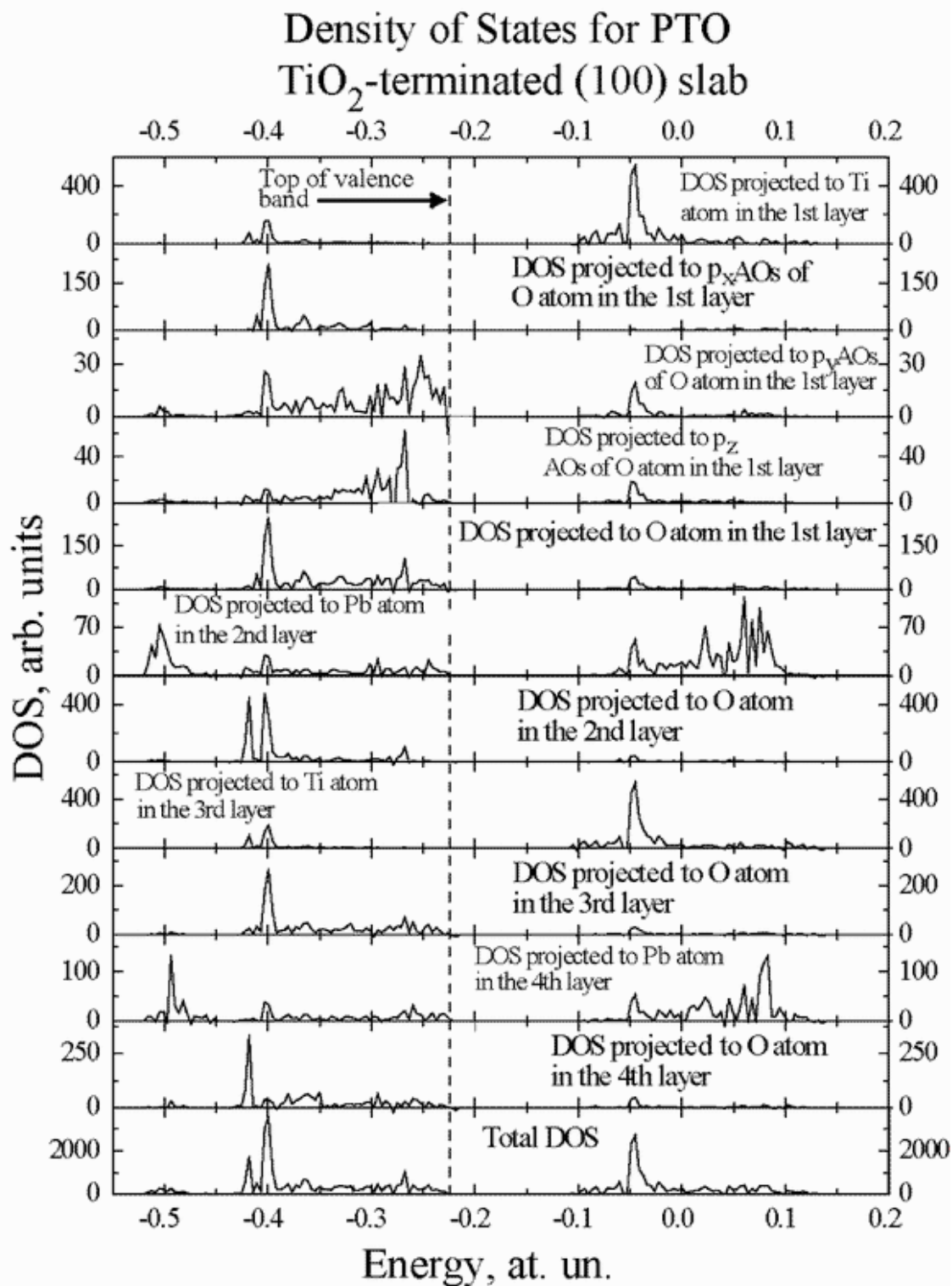


Figure 17: Total and projected DOS for the PTO TiO₂-terminated surface.

15, 16, 17, and Table 11). The narrowest gap of both, bulk and surface band structures corresponds to the transition between Γ and X points of the Brillouin zone. In the bulk, the VB top is formed significantly by Pb 6s AOs (which also make the main contribution to the VB *bottom*). The bulk CB bottom consist of Ti 3d AOs, as in two other perovskites. Surprisingly, the optical band gaps in PbO-terminated surfaces are not smaller, as in BTO and STO, but even a little bit increases (up to 2.96 eV with respect to 2.87 in the bulk). The VB top in the PbO-terminated surface consists of a mixture of Pb 6s and O 2p AOs from a third layer, whereas the CB bottom is formed by Ti 3d AOs from a subsurface layer.

The VB top for the TiO₂-terminated PTO(001) surface at the X point consists of a mixture of the O 2p and Pb 6s AOs from *both* surface and central layers. Moreover, the main contribution comes from the orbitals of *central* atoms. The CB bottom for the TiO₂-terminated PTO consists mainly of the Ti 3d AOs from a third layer.

The band structure calculated for the asymmetrical PTO slab shows a mixture of the band structures of the two symmetrical slabs, as it was observed for STO and BTO.

4 Conclusions

Using hybrid DFT-HF B3PW method, we calculated the surface relaxation and the electronic structure of the two possible terminations of the (001) surfaces for STO, BTO and PTO perovskite crystals. The data obtained for the surface structure are in good agreement with available results of theoretical *ab initio* calculations and with experimental data. The computed relaxed surface energies are quite low, 1-1.5 eV per unit cell. This indicates that the surfaces with both termination are quite stable, in agreement with ideas of a “weak polarity” [2, 47, 48] and existing experiments. The analysis of the atomic dipole moments shows that the cations on the AO-terminated surfaces reveal the strong electronic polarization along the z -axis. The calculated difference electron density maps and bond populations demonstrate an increase of the Ti-O bond covalency near the surfaces, and additionally a weak covalency (polarization) of the Pb-O bond on the PbO terminated surface.

The observed absence of the surface electronic states in the upper VB for the AO-terminated (001) surfaces and considerable (0.5 eV) reduction of the gap for the TiO₂-terminated surface of all three perovskites are important factor for the future treatment of the electronic structure of surface defects on perovskite surfaces, as well as adsorption and surface diffusion of atoms and small molecules, which is relevant for catalysis, fuel cells, and microelectronics.

Acknowledgements

SP was partly supported by DFG. Authors are indebted to R. Evarestov, G. Borstel, and R. Eglitis for numerous discussions.

References

- [1] M. E. Lines, A. M. Glass, Principles and Applications of Ferroelectrics and Related Materials, Clarendon Press, Oxford, 1977.
- [2] C. Noguera, Physics and Chemistry at Oxide Surfaces, Cambridge University Press, New-York, 1996.
- [3] V. E. Henrick, P. A. Cox, The Surface Science of Metal Oxides, Cambridge University Press, New-York, 1994.
- [4] J. F. Scott, Ferroelectric Memories, Advanced Microelectronics 3, Springer, Berlin, 2000.
- [5] N. Bickel, G. Schmidt, K. Heinz, K. Müller, Ferroelectric relaxation of the $\text{SrTiO}_3(100)$ surface, Phys. Rev. Lett. 62 (17) (1989) 2009–2011.
- [6] T. Hikita, T. Hanada, M. Kudo, M. Kawai, Structure and electronic state of the TiO_2 and SrO terminated $\text{SrTiO}_3(100)$ surfaces, Surf. Sci. 287/288 (1993) 377–381.
- [7] A. Ikeda, T. Nishimura, T. Morishita, Y. Kido, Surface relaxation and rumpling of TiO_2 -terminated $\text{SrTiO}_3(001)$ determined by medium energy ion scattering, Surf. Sci. 433-435 (1999) 520–524.
- [8] G. Charlton, S. Brennan, C. A. Muryn, R. McGrath, D. Norman, T. S. Turner, G. Thorthon, Surface relaxation of $\text{SrTiO}_3(001)$, Surf. Sci. 457 (2000) L376–L380.
- [9] P. A. W. van der Heide, Q. D. Jiang, Y. S. Kim, J. W. Rabalais, X-ray photoelectron spectroscopic and ion scattering study of the $\text{SrTiO}_3(001)$ surface, Surf. Sci. 473 (2001) 59–70.
- [10] W. Maus-Friedrichs, M. Frerichs, A. Gunhold, S. Krischok, V. Kempter, G. Bihlmayer, The characterization of $\text{SrTiO}_3(001)$ with MIES, UPS(HeI) and first-principles calculations, Surf. Sci. 515 (2002) 499–506.

- [11] S. Kimura, J. Yamauchi, M. Tsukada, S. Watanabe, First-principles study on electronic structure of the (001) surface of SrTiO_3 , *Phys. Rev. B* 51 (16) (1995) 11049–11054.
- [12] R. E. Cohen, Periodic slab LAPW computations for ferroelectric BaTiO_3 , *J. Phys. Chem. Solids* 57 (10) (1996) 1393–1396.
- [13] R. E. Cohen, Surface effects in ferroelectrics: periodic slab computations for BaTiO_3 , *Ferroelectrics* 194 (1997) 323–342.
- [14] J. Padilla, D. Vanderbilt, *Ab initio* study of BaTiO_3 surfaces, *Phys. Rev. B* 56 (3) (1997) 1625–1631.
- [15] J. Padilla, D. Vanderbilt, *Ab initio* study of SrTiO_3 surfaces, *Surf. Sci.* 418 (1998) 64–70.
- [16] B. Meyer, J. Padilla, D. Vanderbilt, *Faraday Discussions 114: The Surface Science of Metal Oxides*, Royal Society of Chemistry, London, 1999, Ch. Theory of PbTiO_3 , BaTiO_3 , and SrTiO_3 surfaces, pp. 395–405.
- [17] X. Y. Xue, C. L. Wang, W. L. Zhong, The atomic and electronic structure of the TiO_2 and BaO -terminated $\text{BaTiO}_3(001)$ surfaces in a paraelectric phase, *Surf. Sci.* 550 (2004) 73–78.
- [18] F. Cora, C. R. A. Catlow, *Faraday Discussions 114: The Surface Science of Metal Oxides*, Royal Society of Chemistry, London, 1999, Ch. QM investigations on perovskite-structured transition metal oxides: bulk, surfaces and interfaces, pp. 421–442.
- [19] C. Cheng, K. Kunc, M. H. Lee, Structural relaxation and longitudinal dipole moment of $\text{SrTiO}_3(001)$ (1×1) surface, *Phys. Rev. B* 62 (15) (2000) 10409–10418.
- [20] S. Tinte, M. D. Stachiotti, Atomistic simulation of surface effects in BaTiO_3 , *AIP. conf. proc.* 535 (2000) 273–282.
- [21] S. Tinte, M. D. Stachiotti, Surface effects and ferroelectric phase transitions in BaTiO_3 ultrathin films, *Phys. Rev. B* 64 (2001) 235403.
- [22] C. Pisani (Ed.), *Quantum-Mechanical Ab-initio Calculations of the Properties of Crystalline Materials*, Vol. 67 of *Lecture Notes in Chemistry*, Springer, Berlin, 1996.

- [23] L. A. Curtiss, K. Raghavachari, P. C. Redfern, J. A. Pople, Assessment of Gaussian-2 and density functional theories for the computation of enthalpies of formation, *J. Chem. Phys.* 106 (3) (1997) 1063–1079.
- [24] L. A. Curtiss, P. C. Redfern, K. Raghavachari, J. A. Pople, Assessment of Gaussian-2 and density functional theories for the computation of ionization potentials and electron affinities, *J. Chem. Phys.* 109 (1) (1998) 42–55.
- [25] J. Muscat, A. Wander, N. M. Harrison, On the prediction of band gaps from hybrid functional theory, *Chem. Phys. Lett.* 342 (2001) 397–401.
- [26] S. Piskunov, E. Heifets, R. I. Eglitis, G. Borstel, Bulk properties and electronic structure of SrTiO_3 , BaTiO_3 and PbTiO_3 perovskites: an *ab initio* HF/DFT study, *Comp. Mat. Sci.* 29 (2004) 165–178.
- [27] E. Heifets, R. I. Eglitis, E. A. Kotomin, J. Maier, G. Borstel, First-principles calculations for $\text{SrTiO}_3(100)$ surface structure, *Surf. Sci.* 513 (2002) 211–220.
- [28] E. Heifets, E. A. Kotomin, J. Maier, Semi-empirical simulations of surface relaxation for perovskite titanates, *Surf. Sci.* 462 (2000) 19–35.
- [29] E. Heifets, R. I. Eglitis, E. A. Kotomin, J. Maier, G. Borstel, *Ab initio* modeling of surface structure for SrTiO_3 perovskite crystals, *Phys. Rev. B* 64 (2001) 235417.
- [30] E. A. Kotomin, R. I. Eglitis, J. Maier, E. Heifets, Calculations of the atomic and electronic structure for SrTiO_3 perovskite thin films, *Thin Solid Films* 400 (2001) 76–80.
- [31] G. Borstel, R. I. Eglitis, E. A. Kotomin, E. Heifets, Modelling of defects and surfaces in perovskite ferroelectrics, *Phys. Stat. Sol. (b)* 236 (2) (2003) 253–264.
- [32] V. R. Saunders, R. Dovesi, C. Roetti, M. Causa, N. M. Harrison, R. Orlando, C. M. Zicovich-Wilson, *CRYSTAL’98 User’s Manual*, Universita di Torino, Torino (1998).
- [33] <http://www.chimifm.unito.it/teorica/crystal/crystal.html>.
- [34] <http://www.cse.clrc.ac.uk/cmrg/crystal>.
- [35] A. D. Becke, Density-functional thermochemistry. III. the role of exact exchange, *J. Chem. Phys.* 98 (7) (1993) 5648–5652.

- [36] J. P. Perdew, Y. Wang, Accurate and simple density functional for the electronic exchange energy: Generalized gradient approximation, *Phys. Rev. B* 33 (12) (1986) 8800–8802.
- [37] J. P. Perdew, Y. Wang, Erratum: Accurate and simple density functional for the electronic exchange energy: Generalized gradient approximation, *Phys. Rev. B* 40 (5) (1989) 3399.
- [38] J. P. Perdew, Y. Wang, Accurate and simple analytic representation of the electron-gas correlation energy, *Phys. Rev. B* 45 (23) (1992) 13244–13249.
- [39] P. J. Hay, W. R. Wadt, *Ab initio* effective core potentials for molecular calculations. Potentials for the transition metal atoms Sc to Hg, *J. Chem. Phys.* 82 (1) (1984) 270–283.
- [40] P. J. Hay, W. R. Wadt, *Ab initio* effective core potentials for molecular calculations. Potentials for main group elements Na to Bi, *J. Chem. Phys.* 82 (1) (1984) 284–298.
- [41] P. J. Hay, W. R. Wadt, *Ab initio* effective core potentials for molecular calculations. Potentials for K to Au including the outermost core orbitals, *J. Chem. Phys.* 82 (1) (1984) 299–310.
- [42] H. J. Monkhorst, J. D. Pack, Special points for Brillouin-zone integrations, *Phys. Rev. B* 13 (12) (1976) 5188–5192.
- [43] T. Bredow, R. A. Evarestov, K. Jug, Implementation of the Cyclic Cluster Model in Hartree-Fock LCAO calculations of crystalline systems, *Phys. Stat. Solidi. (b)* 222 (2000) 495–516.
- [44] K. H. Hellwege, A. M. Hellwege (Eds.), *Ferroelectrics and Related Substances*, Vol. 3 of New Series, Landolt-Bornstein, Springer Verlag, Berlin, 1969, group III.
- [45] B. G. Shirane, R. Repinsky, B. C. Frazer, X-ray and neutron diffraction study of ferroelectric PbTiO_3 , *Acta. Cryst.* 9 (1956) 131–140.
- [46] W. H. Press, S. A. Teukolsky, W. T. Vetterling, B. P. Flannery, *Numerical Recipes in Fortran77*, 2nd Edition, Cambridge Univ. Press, Cambridge, MA, 1997.
- [47] P. W. Tasker, The stability of ionic crystal surfaces, *J. Phys. C: Solid State Phys.* 12 (1979) 4977–4984.

- [48] J. Goniakowski, C. Noguera, The concept of weak polarity: an application to the $\text{SrTiO}_3(001)$ surface, *Surf. Sci.* 365 (1996) L657–L662.
- [49] R. A. Evarestov, V. P. Smirnov, D. E. Usvyat, Local properties of the electronic structure of cubic SrTiO_3 , BaTiO_3 and PbTiO_3 crystals in Wannier-type function approach, is submitted to *Solid State Communications* (2003).
- [50] S. H. Wemple, Polarization fluctuations and the optical-absorption edge in BaTiO_3 , *Phys. Rev. B* 2 (7) (1970) 2679–2689.
- [51] C. H. Peng, J. F. Chang, S. Desu, *Mater. Res. Soc. Symp. Proc.* 243 (1992) 21.
- [52] K. van Benthem, C. Elsaesser, R. H. French, Bulk electronic structure of SrTiO_3 : Experiment and theory, *J. Appl. Phys.* 90 (12) (2001) 6156–6164.
- [53] S. de Lasaro, E. Longo, J. R. Sambrano, A. Beltran, Structural and electronic properties of PbTiO_3 slabs: a DFT periodic study, *Surf. Sci.* 552 (2004) 149–159.